Phased-Array-Based Sub-Nyquist Sampling for Joint Wideband Spectrum Sensing and Direction-of-Arrival Estimation

Feiyu Wang, Jun Fang, *Member, IEEE*, Huiping Duan, and Hongbin Li, *Senior Member, IEEE*

***Abstract*—In this paper, we study the problem of joint wideband spectrum sensing and direction-of-arrival (DoA) estimation in a sub-Nyquist sampling framework. Specifically, considering a scenario where a number of uncorrelated narrow-band signals spread over a wide (say, several GHz) frequency band, our objective is to estimate the carrier frequencies and the DoAs associated with the narrow-band sources, as well as reconstruct the power spectra of these narrow-band signals. To overcome the sampling rate bottleneck for wideband spectrum sensing, we propose a new phased-array-based sub-Nyquist sampling architecture with flexible time delays, where a uniform linear array is employed and the received signal at each antenna is delayed by a flexible amount of time and then sampled by a synchronized low-rate analog–digital converter. Based on the collected sub-Nyquist samples, we calculate a set of cross-correlation matrices with different time lags, and develop a CANDECOMP/PARAFAC decomposition-based method for joint DoA, carrier frequency, and power spectrum recovery. Conditions for perfect recovery of the associated parameters and the power spectrum are analyzed. Simulation results show that our proposed method presents a clear performance advantage over existing methods, and achieves an estimation accuracy close to the associated Cramér–Rao bounds using only a small number of data samples.**

***Index Terms*—Joint wideband spectrum sensing and direction-of-arrival (DoA) estimation, compressed sensing, CANDECOMP/PARAFAC (CP) decomposition.**

Manuscript received May 21, 2018; revised September 23, 2018; accepted September 26, 2018. Date of publication October 10, 2018; date of current version October 22, 2018.The associate editor coordinating the review of this manuscript and approving it for publication was Dr. Fabiola Colone. This work was supported in part by the National Science Foundation of China under Grants 61522104, 61871091, and U1530154 and in part by the National Science Foundation under Grants ECCS-1408182 and ECCS-1609393. This paper was presented in part at the IEEE International Workshop on Computational Advances in Multi-Sensor Adaptive Processing, Curaçao, Dutch Antilles, December 2017. *(Corresponding author: Jun Fang.)*

F. Wang and J. Fang are with the National Key Laboratory of Science and Technology on Communications, and the Center for Intelligent Networking and Communications, University of Electronic Science and Technology of China, Chengdu 611731, China (e-mail: fywang.ee@outlook.com; JunFang@uestc.edu.cn).

H. Duan is with the School of Information and Communication Engineering, University of Electronic Science and Technology of China, Chengdu 611731, China (e-mail: huipingduan@uestc.edu.cn).

H. Li is with the Department of Electrical and Computer Engineering, Stevens Institute of Technology, Hoboken, NJ 07030 USA (e-mail: Hongbin.Li@stevens.edu).

Color versions of one or more of the figures in this paper are available online at http://ieeexplore.ieee.org.

Digital Object Identifier 10.1109/TSP.2018.2875420

I. Introduction

WIDEBAND spectrum sensing, which aims to identify the frequency locations of a number of *narrowband* transmissions that spread over a wide frequency band, has been of a growing interest in signal processing and cognitive radio communications [1], [2]. It is noteworthy to point out that, although the spectrum under monitoring has a large bandwidth, which is the reason why the term "wideband spectrum sensing" is used in this work, the source signals residing in the wide frequency band are assumed to be narrowband signals. We will justify such an assumption later in our paper. To perform wideband spectrum sensing, a conventional receiver requires to sample the received signal at a Nyquist rate, which may be infeasible if the spectrum under monitoring is very wide, say, reaches several GHz. Also, a high sampling rate results in a large amount of data which place a heavy burden on subsequent storage and processing. One way to overcome this issue is to divide the frequency spectrum under monitoring into a number of separate frequency segments and then sequentially scan these frequency channels. Nevertheless, such a scanning scheme incurs a sensing latency and may fail to capture short-lived signals. To alleviate the sampling rate requirement and accomplish the wideband spectrum sensing task in a one-shot manner without performing channel-by-channel scanning, a variety of sub-Nyquist sampling schemes, e.g. [3]–[6], were developed. The rationale behind such schemes is to exploit the inherent sparsity in the frequency domain and formulate wideband spectrum sensing as a sparse signal recovery problem which, according to the compressed sensing theory [7], [8], can perfectly recover the signal of the entire frequency band based on compressed measurements or sub-Nyquist samples. Furthermore, in [9]–[11], it was shown that it is even possible to perfectly reconstruct the power spectrum without placing any sparse constraint on the wideband spectrum under monitoring.

In some applications such as electronic warfare, one need not only conduct wideband spectrum sensing, but also identify the carrier frequencies and directions-of-arrival (DoAs) associated with the narrowband signals that live within the wide frequency band [12]. Besides, in massive MIMO or millimeter wave systems where signals are transmitted via beamforming techniques, the DoA information would allow a cognitive radio to more efficiently exploit the vacant bands [13]. In [14], [15], ESPRIT-based methods were proposed for joint carrier frequency and DoA estimation. These methods need to perform a high-dimensional singular value decomposition (SVD) and

thus involve a high computational complexity. In [16], a computationally efficient tree-structured frequency-space-frequency (FSF) multiple signal classification (MUSIC) based algorithm was developed to jointly estimate the DoAs and carrier frequencies. All these methods [14]–[16], however, require the signal to be sampled at a Nyquist rate. Recently, with the advent of compressed sensing theories, the sparsity inherent in the spectral and spatial domains was utilized to devise sub-Nyquist sampling-based algorithms for joint wideband spectrum sensing and DoA estimation. Specifically, in [17], a compressed sensing method was developed in a phased array framework, where a multicoset sampling scheme is performed at each antenna to collect non-uniform samples. In practice, the multicoset sampling can be implemented using multiple channels, with each channel delayed by a different time offset and then sampled by a low-rate analog-digital converter (ADC). It is also noteworthy to mention that [17] not only assumes multicoset sampling in time, but also in space, which leads to a sparse array and helps substantially reduce its hardware complexity. In [18], [19], a simplified sub-Nyquist receiver architecture was proposed, in which each antenna output is connected with only two channels, i.e. a direct path and a delayed path. An ESPRIT-based algorithm was then developed for joint DoA, carrier frequency, and signal reconstruction. In addition to the above time delay-based sub-Nyquist receiver architectures, an alternative sub-Nyquist sampling approach, referred to as phased array-based modulated wideband converter (MWC), was proposed in [13], [20] for carrier and DoA estimation. The receiver utilizes an L-shaped array, with each sensor implementing a single channel of the MWC. Recently, another MWC-based sub-Nyquist sampling architecture was proposed in [21], where a two-stage method was developed for joint carrier frequency and DoA estimation.

In this paper, we propose a new sub-Nyquist receiver architecture for joint wideband spectrum sensing and DoA estimation. In our architecture, the received signal at each antenna is delayed by a flexible time shift and then sampled at a sub-Nyquist sampling rate. Compared with existing sub-Nyquist receiver architectures, e.g. [18], [19], [21], our proposed sub-Nyquist scheme is simpler and easier to implement: it requires only one ADC for each antenna output, thus leading to a lower hardware complexity. Also, in our proposed architecture, the time delays can be arbitrarily chosen as long as they satisfy a mild condition, which relaxes the requirement on the accuracy of time delay lines. From the collected sub-Nyquist samples, we calculate a set of cross-correlation matrices with different time lags, based on which a third-order tensor that admits a CANDECOMP/PARAFAC (CP) decomposition can be constructed. We show that the DoAs and the carrier frequencies, along with the power spectra associated with the sources, can be recovered from the factor matrices. The perfect recovery condition is analyzed. Our analysis shows that the overall sampling rate required by our proposed method for perfect recovery is approximately half of that required by other state-of-the-art methods, e.g. [18], [20].

We notice that a CP decomposition-based approach was proposed in [13] for joint DoA and carrier frequency estimation. Different from our work, the construction of the tensor in [13] has to rely on an L-shaped array and exploits the cross-correlations between the two mutually perpendicular sub-arrays. In addition, the PARAFAC analysis in [13] can only help extract the DoA and carrier frequency information, while in our proposed method, the DoA, carrier frequency, and power spectrum associated with each source can be simultaneously recovered from the CP decomposition. It was also brought to our attention that another CP decomposition-based approach was recently proposed in [22]. Nevertheless, there are some important distinctions between our work and theirs. Firstly, different from our receiver architecture, the work [22] employs a multicoset sampling scheme to sample the signal received by each antenna, which involves a higher hardware complexity and requires a precise time control on the time delay lines. Secondly, our work and [22] have very different ideas in constructing their respective third-order tensors. Specifically, the third-order tensor in [22] is constructed from original data samples, whereas ours is constructed from a set of correlation matrices. The use of the statistical information enables our proposed algorithm to accurately estimate the carrier frequency and DoA parameters in a low signal-to-noise regime. Such a merit is particularly useful because wideband receivers usually have to operate in a low signal-to-noise region.

The rest of the paper is organized as follows. In Section II, we provide notations and basics on the CP decomposition. The signal model and related assumptions are discussed in Section III. In Section IV, we propose a new phase-array based sub-Nyquist receiver architecture. A CP decomposition-based method for joint wideband spectrum sensing and DoA estimation is developed in Section V, along with the analysis of the uniqueness of the CP decomposition. The exact recovery condition and the extension to sparse arrays are discussed in Section VI. The CRB analysis is conducted in Section VII. Simulation results are provided in Section VIII, followed by concluding remarks in Section IX.

II. Preliminaries

To make the paper self-contained, we provide a brief review on tensors and the CP decomposition. More details regarding the notations and basics on tensors can be found in [23]. Simply speaking, a tensor is a generalization of a matrix to higher-order dimensions, also known as ways or modes. Vectors and matrices can be viewed as special cases of tensors with one and two modes, respectively. Throughout this paper, we use symbols $\otimes$, $\circ$, and $\odot$ to denote the Kronecker, outer, and Khatri-Rao product, respectively.

Let $\boldsymbol{\mathcal{X}} \in \mathbb{C}^{I_1 \times I_2 \times \cdots \times I_N}$ denote an Nth-order tensor with its $(i_1, \ldots, i_N)$th entry denoted by $\mathcal{X}_{i_1 \cdots i_N}$. Here the order N of a tensor is the number of dimensions. Fibers are higher-order analogues of matrix rows and columns. The mode-n fibers of $\boldsymbol{\mathcal{X}}$ are I_n-dimensional vectors obtained by fixing every index but i_n. Slices are two-dimensional sections of a tensor, defined by fixing all but two indices. Unfolding or matricization is an operation that turns a tensor into a matrix. The mode-n unfolding of a tensor $\boldsymbol{\mathcal{X}}$, denoted as $\boldsymbol{X}_{(n)}$, arranges the mode-n fibers to be the columns of the resulting matrix. The CP decomposition

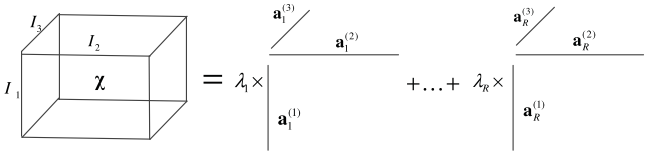

Fig. 1. Schematic of CP decomposition.

decomposes a tensor into a sum of rank-one component tensors (see Fig. 1), i.e.

$$\boldsymbol{\mathcal{X}} = \sum_{r=1}^{R} \lambda_r \boldsymbol{a}_r^{(1)} \circ \boldsymbol{a}_r^{(2)} \circ \cdots \circ \boldsymbol{a}_r^{(N)} \tag{1}$$

where $\boldsymbol{a}_r^{(n)} \in \mathbb{C}^{I_n}$, the minimum achievable R is referred to as the rank of the tensor, and $\boldsymbol{A}^{(n)} \triangleq [\boldsymbol{a}_1^{(n)} \ \ldots \ \boldsymbol{a}_R^{(n)}] \in \mathbb{C}^{I_n \times R}$ denotes the factor matrix along the n-th mode. Elementwise, we have $\mathcal{X}_{i_1 i_2 \cdots i_N} = \sum_{r=1}^{R} \lambda_r a_{i_1 r}^{(1)} a_{i_2 r}^{(2)} \ldots a_{i_N r}^{(N)}$. The mode-$n$ unfolding of $\boldsymbol{\mathcal{X}}$ can be expressed as $\boldsymbol{X}_{(n)} = \boldsymbol{A}^{(n)} \boldsymbol{\Lambda} (\boldsymbol{A}^{(N)} \odot \cdots \boldsymbol{A}^{(n+1)} \odot \boldsymbol{A}^{(n-1)} \odot \cdots \boldsymbol{A}^{(1)})^T$, where $\boldsymbol{\Lambda} \triangleq \text{diag}(\lambda_1, \ldots, \lambda_R)$.

III. Signal Model

Consider a scenario in which K uncorrelated, wide-sense stationary, and far-field narrowband signals spreading over a wide frequency band impinge on a wideband uniform linear array (ULA) with N receive antennas, where we assume $N > K$. Let $s(t)$ denote the combination of the K narrowband signals in the time domain. $s(t)$ can be expressed as

$$s(t) = \sum_{k=1}^{K} s_k(t) e^{j\omega_k t} \tag{2}$$

where $s_k(t)$ and $\omega_k \in \mathbb{R}^+$ denote the complex baseband signal and the carrier frequency (in radians per second) of the kth source signal, respectively. Each source signal $s_k(t)$ is associated with an unknown azimuth DoA $\theta_k \in [0, \pi)$. We have the following assumptions regarding the source signals:

- A1 The multi-band signal $s(t)$ is bandlimited to $\mathcal{F} = [0, f_{\text{nyq}}]$.
- A2 The K source signals $\{s_k(t)\}$ are assumed to be mutually uncorrelated, wide-sense stationary, and bandlimited to $[-B/2, B/2]$, i.e. $B_k \leq B, \forall k$, where B_k denotes the bandwidth of the kth source signal.
- A3 The K source signals $\{s_k(t)\}$ are assumed to be narrowband signals. In other words, the inverse bandwidth of each signal is much larger than the time it takes to travel across the array, i.e.

$$1/B \gg (N-1)d/C \tag{3}$$

  where d denotes the distance between adjacent antennas and C is the speed of light.
- A4 Sources either have distinct carrier frequencies $\{\omega_k\}$ or distinct DoAs $\{\theta_k\}$, i.e. for any two source signals, we have $(\theta_i, \omega_i) \neq (\theta_j, \omega_j), \forall i \neq j$.

Assumption A4 is assumed to make signals distinguished from one another. Note that this assumption is less restrictive than the one made in other works, e.g. [18], [20], which, in order to remove the source ambiguity, require the quantity $\omega_k \cos(\theta_k)$ to be mutually different for different signals, i.e.

$$\omega_i \cos(\theta_i) \neq \omega_j \cos(\theta_j) \quad \forall i \neq j \tag{4}$$

After collecting the received signal at the array, our objective is to jointly estimate the DoAs $\{\theta_k\}$, the carrier frequencies $\{\omega_k\}$, as well as the power spectra associated with the K source signals. To accomplish this task, we, in the following, propose a new phased-array based sub-Nyquist receiver architecture.

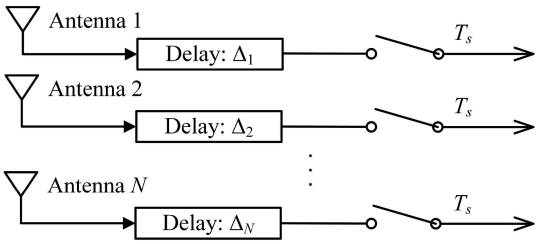

Fig. 2. Proposed phased-array based sub-Nyquist sampling architecture with flexible time delays (PASS-FD).

IV. Proposed Sub-Nyquist Receiver Architecture

A. Proposed Receiver Architecture

In our receiver architecture, the received signal at each antenna is delayed by a pre-specified factor Δ_n and then sampled by a synchronous ADC with a sampling rate of $f_s = 1/T_s$, where $f_s \ll f_{\text{nyq}}$. We have the following assumptions regarding the delay factors and the sampling rate:

- A5 The time delay factors $\{\Delta_n\}$ can take arbitrary values as long as the following condition is satisfied

$$0 < (\Delta_{n+2} - 2\Delta_{n+1} + \Delta_n) f_{\text{nyq}} \leq 1 \tag{5}$$

  for a certain $n \in \{1, \ldots, N-2\}$, and meanwhile they are small enough

$$1/B \gg \max_n \{\Delta_n\} \tag{6}$$

  such that the approximation in (7) holds valid.
- A6 The sampling rate f_s is no less than the bandwidth of the narrowband source signal which has the largest bandwidth among all sources, i.e. $f_s \geq B$.

As will be shown later in our paper, (5) is essential to identify the unknown carrier frequencies. The proposed receiver architecture, termed as the Phased-Array based Sub-Nyquist Sampling architecture with Flexible time Delays (PASS-FD), is illustrated in Fig. 2. The analog signal observed by the nth antenna can be expressed as

$$\begin{aligned} x_n(t) &= \sum_{k=1}^{K} s_k(t - (n-1)\tau_k - \Delta_n) \\ &\qquad \times e^{j\omega_k (t - (n-1)\tau_k - \Delta_n)} + w_n(t) \\ &\approx \sum_{k=1}^{K} s_k(t) e^{j\omega_k (t - (n-1)\tau_k - \Delta_n)} + w_n(t) \end{aligned} \tag{7}$$

where $w_n(t)$ represents the additive white Gaussian noise with zero mean and variance σ^2, and τ_k denotes the delay between two adjacent sensors for a plane wave arriving in the direction θ_k and is given by

$$\tau_k = d\cos\theta_k / C \tag{8}$$

The approximation in (7) is due to the narrowband assumption (3) and the relatively small values of the time delay factors. In fact, from (3) and (6), we have

$$\begin{aligned} 1/B &\gg \max_n\{\Delta_n\} + (N-1)d/C \\ &> \max_n\{\Delta_n\} + (N-1)\tau_k \end{aligned} \tag{9}$$

Since the quantity $(n-1)\tau_k + \Delta_n$ is much smaller than the inverse of the bandwidth of the signal, $s_k(t-(n-1)\tau_k - \Delta_n)$ can be well approximated by $s_k(t)$.

We adopt the following assumption for the distance between two adjacent antennas

A7 The distance between two adjacent antennas d satisfies $d < C/(2f_{\text{nyq}})$, where C is the speed of light.

As will be shown later in our paper, this assumption is essential for the recovery of the DoAs. Also, from $d < C/(2f_{\text{nyq}})$, it can be easily verified that the narrowband condition (3) is equivalent to

$$f_{\text{nyq}}/B \gg (N-1)/2 \tag{10}$$

The above inequality implies that a signal can be considered as a narrowband signal if its bandwidth is relatively small as compared with f_{nyq}, the range of the frequency band under monitoring, which is usually the case for wideband spectrum sensing and electronic warfare surveillance applications.

In practice, only the real part of $x_n(t)$ is observed and sampled. Nevertheless, the corresponding imaginary part $\Im[x_n(t)]$ can be retrieved from the real part $\Re[x_n(t)]$ by passing the signal through a finite impulse response (FIR) Hilbert transformer. The complex analytic signal can also be roughly approximated by computing the discrete Fourier transform (DFT) of the output of each antenna and throwing away the negative frequency portion of the spectrum [12].

B. Relation to and Distinction From Existing Architectures

We notice that a time delay-based sub-Nyquist architecture was also introduced in [17]–[19]. Nevertheless, there are two key distinctions between our architecture and theirs. Firstly, our architecture has a simpler structure with only N delay channels, whereas the architecture proposed in [18] (see Fig. 3(a)) requires $2N$ channels in total, in which each antenna output passes through two channels, namely, a direct path and a delayed path. As a consequence, the number of required ADCs for the architecture [18] is twice the number of ADCs for our architecture. In [19], a modified architecture was proposed based on [18]. It, however, still requires $2N$ channels, with an N-channel delay network added to the first antenna. Secondly, for our proposed architecture, the time delays can take arbitrary values as long as the mild condition (5) is satisfied. In contrast, for other architectures, e.g. [17]–[19], a precise time control is required

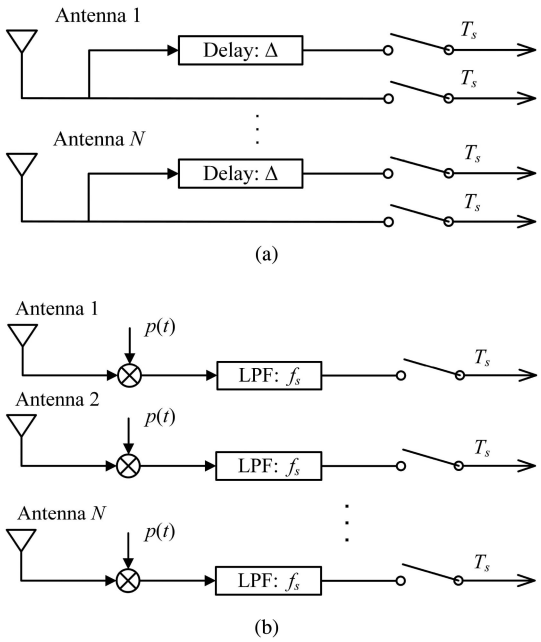

Fig. 3. Existing sub-Nyquist receiver architectures. (a) Sub-Nyquist sampling architecture proposed in [18]. (b) Sub-Nyquist sampling architecture proposed in [20].

such that the time delays across different channels are strictly identical [18], [19], or the time delays must be integer multiples of the Nyquist sampling interval [17]. Due to the inaccuracy caused by the time shift elements, maintaining accurate time delays on the order of the Nyquist sampling interval is difficult. The inaccuracy in these delays will impair the recovery performance. Our architecture is free from this issue because it allows more flexible time delays and we can use the actual time delays measured in practice for our proposed recovery algorithm.

In [13], [20], a phased-array MWC-based sub-Nyquist sampling architecture (see Fig. 3(b)) was proposed for joint wideband spectrum sensing and DoA estimation, in which an L-shaped array is adopted, and the output of each sensor is multiplied by a same periodic pseudo-random sequence, low-pass filtered and then sampled at a low rate. Compared to the phased-array MWC-based sub-Nyquist sampling architecture, our proposed delay-based scheme is much simpler to implement. In [24], it is argued that the delay-based architectures suffer two major disadvantages which include the need for high-precision delay lines as well as specialized ADCs with high analog bandwidth. Nevertheless, as discussed above, our proposed architecture, different from other delay-based schemes [17]–[19], has a relaxed requirement on the precision of delay lines. Regarding the latter issue, we would like to clarify that many standard low-rate ADCs actually have a relatively large analog (full-power) bandwidth.[1] For example, the commercial ADC device ADS4122 has a sampling rate of 65 MHz, while its analog bandwidth is up to 800 MHz. Some other low-rate ADCs with affordable prices, such as ADC12D500, have an analog

[1]Here the analog bandwidth is an important specification of ADCs and determines the highest frequency that can be handled by the device.

bandwidth up to 2.7 GHz. Also, these ADCs usually have a nearly flat spectral response within its analog bandwidth. On the other hand, we agree that standard low-rate ADCs, when operating on its full analog bandwidth, may bring some distortion due to the hardware imperfections. Such an issue should be taken into account in system design and algorithmic development.

V. Proposed CP Decomposition-Based Method

We first calculate the cross-correlation between two sensor outputs $x_m(t_1)$ and $x_n(t_2)$. Recalling Assumption A2, we have

$$R^x_{mn}(t_1,t_2) = \mathbb{E}\left[x_m(t_1)x_n^*(t_2)\right] = \sum_{k=1}^{K} R^s_k(t_1,t_2)a_{mk}a^*_{nk} + R^w_{mn}(t_1,t_2) \quad (11)$$

where

$$R^s_k(t_1,t_2) \triangleq \mathbb{E}\left[s_k(t_1)e^{j\omega_k t_1}\, s_k^*(t_2)e^{-j\omega_k t_2}\right] \quad (12)$$

denotes the autocorrelation of the k-th modulated source signal, $R^w_{mn}(t_1,t_2) \triangleq \mathbb{E}\left[w_m(t_1)w_n^*(t_2)\right]$ represents the autocorrelation of the additive noise and

$$a_{nk} \triangleq e^{-j((n-1)\tau_k\omega_k + \Delta_n\omega_k)} \quad (13)$$

Since the source signals are wide-sense stationary, the autocorrelation $R^s_k(t_1,t_2)$ depends only on the time difference $t_1 - t_2$. As a result, the cross-correlation of the sensor outputs $R^x_{mn}(t_1,t_2)$ depends on the time difference $t_1 - t_2$ as well. Let T_s denote the sampling interval of the ADCs. The time difference has to be an integer multiple of the sampling interval, i.e. $t_1 - t_2 = lT_s$ for $l = -L,\ldots,L$. For notational convenience, we define $r^x_{m,n}(l) \triangleq R^x_{mn}(t+lT_s,t)$, $r^s_k(l) \triangleq R^s_k(t+lT_s,t)$ and $r^w_{m,n}(l) \triangleq R^w_{mn}(t+lT_s,t)$. We can therefore express (11) as a discrete-time form:

$$r^x_{m,n}(l) = \sum_{k=1}^{K} r^s_k(l)a_{mk}a^*_{nk} + r^w_{m,n}(l) \quad (14)$$

for $l = -L,\ldots,L$ and $m,n = 1,\ldots,N$.

Our objective is to recover the DoAs $\{\theta_k\}$, the carrier frequencies $\{\omega_k\}$, as well as the power spectra associated with the K source signals based on the second-order statistics $\{r^x_{m,n}(l)\}$. For each time lag l, we can construct a correlation matrix $\boldsymbol{R}^x(l)$ with its (m,n)th entry given by $r^x_{m,n}(l)$. Also, it can be easily verified that

$$\boldsymbol{R}^x(l) = \sum_{k=1}^{K} r^s_k(l)\boldsymbol{a}_k\boldsymbol{a}_k^H + \boldsymbol{R}^w(l) \quad (15)$$

where $\boldsymbol{R}^w(l)$ denotes the cross-correlation matrix of the additive noise with its (m,n)th entry given by $r^w_{m,n}(l)$, and

$$\boldsymbol{a}_k \triangleq [a_{1k}\ \ a_{2k}\ \ \ldots\ \ a_{Nk}]^T \quad (16)$$

Since a set of cross-correlation matrices $\{\boldsymbol{R}^x(l)\}_{l=-L}^{L}$ are available, we can naturally express this set of correlation matrices by a third-order tensor $\boldsymbol{\mathcal{R}}^x \in \mathbb{C}^{(2L-1)\times N\times N}$ whose three modes respectively stand for the time lag l and the antenna indices, and its (l,m,n)-th entry given by $r^x_{m,n}(l)$. Notice from (15) that each slice of the tensor $\boldsymbol{\mathcal{R}}^x$, $\boldsymbol{R}^x(l)$, is a weighted sum of a common set of rank-one outer products. The tensor $\boldsymbol{\mathcal{R}}^x$ thus admits a CP decomposition which decomposes a tensor into a sum of rank-one component tensors, i.e.

$$\boldsymbol{\mathcal{R}}^x = \sum_{k=1}^{K} \boldsymbol{r}_k \circ \boldsymbol{a}_k \circ \boldsymbol{a}_k^* + \boldsymbol{\mathcal{R}}^w \quad (17)$$

where $\circ$ denotes the outer product, $\boldsymbol{\mathcal{R}}^w \in \mathbb{C}^{(2L-1)\times N\times N}$ with its (l,m,n)-th entry given by $r^w_{m,n}(l)$, and $\boldsymbol{r}_k \triangleq [r^s_k(-L)\ \ldots\ r^s_k(L)]^T$.

Define $\boldsymbol{R} \triangleq [\boldsymbol{r}_1\ \ \ldots\ \ \boldsymbol{r}_K]$ and

$$\boldsymbol{A} \triangleq [\boldsymbol{a}_1\ \ \ldots\ \ \boldsymbol{a}_K] \quad (18)$$

The three matrices $\{\boldsymbol{R},\boldsymbol{A},\boldsymbol{A}^*\}$ are referred to as factor matrices associated with the noiseless version of $\boldsymbol{\mathcal{R}}^x$. We see that the information about the parameters $\{\theta_k,\omega_k\}$ as well as the power spectra can be extracted from the factor matrices. Motivated by this observation, we propose a two-stage method which consists of a CP decomposition stage whose objective is to estimate the factor matrices and a parameter estimation stage whose objective is to jointly recover the DoAs, carrier frequencies, and the power spectra of sources based on the estimated factor matrices.

A. CP Decomposition

We first consider the scenario where the number of sources, K, is known or estimated *a priori* via some conventional techniques such as the Akaike information criterion (AIC) [25]. Clearly, the CP decomposition can be accomplished by solving the following optimization problem

$$\min_{\hat{\boldsymbol{R}},\hat{\boldsymbol{A}}} \left\| \boldsymbol{\mathcal{R}}^x - \sum_{k=1}^{K} \hat{\boldsymbol{r}}_k \circ \hat{\boldsymbol{a}}_k \circ \hat{\boldsymbol{a}}_k^* \right\|_F^2 \quad (19)$$

where $\hat{\boldsymbol{R}} = [\hat{\boldsymbol{r}}_1\ \ \ldots\ \ \hat{\boldsymbol{r}}_K]$, $\hat{\boldsymbol{A}} = [\hat{\boldsymbol{a}}_1\ \ \ldots\ \ \hat{\boldsymbol{a}}_K]$, and $\|\cdot\|_F$ denotes the Frobenius norm. On the other hand, note that the CP decomposition is unique under a mild condition. Therefore we can use a new variable $\hat{\boldsymbol{b}}_k$ to replace $\hat{\boldsymbol{a}}_k^*$, which leads to

$$\min_{\hat{\boldsymbol{R}},\hat{\boldsymbol{A}},\hat{\boldsymbol{B}}} \left\| \boldsymbol{\mathcal{R}}^x - \sum_{k=1}^{K} \hat{\boldsymbol{r}}_k \circ \hat{\boldsymbol{a}}_k \circ \hat{\boldsymbol{b}}_k \right\|_F^2 \quad (20)$$

where $\hat{\boldsymbol{B}} \triangleq [\hat{\boldsymbol{b}}_1\ \ \ldots\ \ \hat{\boldsymbol{b}}_K]$. The above optimization can be efficiently solved through an alternating least squares (ALS) procedure which alternatively updates one of the factor matrices to minimize the data fitting error while keeping the other two factor matrices fixed:

$$\widehat{\boldsymbol{R}}^{(t)} = \arg\min_{\boldsymbol{R}} \left\| (\boldsymbol{R}^x_{(1)})^T - (\widehat{\boldsymbol{B}}^{(t-1)} \odot \widehat{\boldsymbol{A}}^{(t-1)})\boldsymbol{R}^T \right\|_F^2 \quad (21)$$

$$\widehat{\boldsymbol{A}}^{(t)} = \arg\min_{\boldsymbol{A}} \left\| (\boldsymbol{R}^x_{(2)})^T - (\widehat{\boldsymbol{B}}^{(t-1)} \odot \widehat{\boldsymbol{R}}^{(t)})\boldsymbol{A}^T \right\|_F^2 \quad (22)$$

$$\widehat{\boldsymbol{B}}^{(t)} = \arg\min_{\boldsymbol{B}} \left\| (\boldsymbol{R}^x_{(3)})^T - (\widehat{\boldsymbol{A}}^{(t)} \odot \widehat{\boldsymbol{R}}^{(t)})\boldsymbol{B}^T \right\|_F^2 \quad (23)$$

where $\boldsymbol{R}^x_{(n)}$ denotes the mode-n unfolding of $\boldsymbol{\mathcal{R}}^x$.

If the knowledge of the number of sources, K, is unavailable, more sophisticated CP decomposition techniques (e.g. [26]–[28]) can be employed to jointly estimate the model order and the factor matrices. The basic idea is to use low rank-promoting priors or functions to automatically determine the CP rank of the tensor. In [26], when the CP rank, K, is unknown, the following optimization was employed for CP decomposition

$$\min_{\hat{\boldsymbol{R}},\hat{\boldsymbol{A}},\hat{\boldsymbol{B}}} \quad \|\boldsymbol{\mathcal{R}}^x - \boldsymbol{\mathcal{X}}\|_F^2 + \mu\Big(\mathrm{tr}(\hat{\boldsymbol{R}}\hat{\boldsymbol{R}}^H) + \mathrm{tr}(\hat{\boldsymbol{A}}\hat{\boldsymbol{A}}^H) + \mathrm{tr}(\hat{\boldsymbol{B}}\hat{\boldsymbol{B}}^H)\Big)$$

$$\text{s.t.} \quad \boldsymbol{\mathcal{X}} = \sum_{k=1}^{\hat{K}} \hat{\boldsymbol{r}}_k \circ \hat{\boldsymbol{a}}_k \circ \hat{\boldsymbol{b}}_k \tag{24}$$

where $\hat{K} \gg K$ denotes an overestimated CP rank, μ is a regularization parameter to control the tradeoff between low-rankness and the data fitting error, $\hat{\boldsymbol{R}} = [\hat{\boldsymbol{r}}_1 \ \ldots \ \hat{\boldsymbol{r}}_{\hat{K}}]$, $\hat{\boldsymbol{A}} = [\hat{\boldsymbol{a}}_1 \ \ldots \ \hat{\boldsymbol{a}}_{\hat{K}}]$, and $\hat{\boldsymbol{B}} = [\hat{\boldsymbol{b}}_1 \ \ldots \ \hat{\boldsymbol{b}}_{\hat{K}}]$. The above optimization (24) can still be solved by an ALS procedure [26]. The true CP rank of the tensor, K, can be estimated by removing those negligible rank-one tensor components after convergence.

B. Joint DoA, Carrier Frequency and Power Spectrum Estimation

We discuss how to jointly recover the DoAs, carrier frequencies, and power spectra of sources based on the estimated factor matrices. As shown in the next subsection, the CP decomposition is unique up to scaling and permutation ambiguities under a mild condition. More precisely, the estimated factor matrices and the true factor matrices are related as

$$\hat{\boldsymbol{R}} = \boldsymbol{R}\boldsymbol{\Lambda}_1\boldsymbol{\Pi} + \boldsymbol{E}_1 \tag{25}$$

$$\hat{\boldsymbol{A}} = \boldsymbol{A}\boldsymbol{\Lambda}_2\boldsymbol{\Pi} + \boldsymbol{E}_2 \tag{26}$$

$$\hat{\boldsymbol{B}} = \boldsymbol{A}^*\boldsymbol{\Lambda}_3\boldsymbol{\Pi} + \boldsymbol{E}_3 \tag{27}$$

where $\{\boldsymbol{\Lambda}_1, \boldsymbol{\Lambda}_2, \boldsymbol{\Lambda}_3\}$ are unknown nonsingular diagonal matrices which satisfy $\boldsymbol{\Lambda}_1\boldsymbol{\Lambda}_2\boldsymbol{\Lambda}_3 = \boldsymbol{I}$; $\boldsymbol{\Pi}$ is an unknown permutation matrix; and $\boldsymbol{E}_1$, $\boldsymbol{E}_2$, and $\boldsymbol{E}_3$ denote the estimation errors associated with the three estimated factor matrices, respectively. The permutation matrix $\boldsymbol{\Pi}$ can be ignored as it is common to all three factor matrices. Also, since we have prior knowledge that columns of $\boldsymbol{A}/\sqrt{N}$ have unit norm, the amplitude ambiguity can be estimated and removed, in which case we can write

$$\hat{\boldsymbol{R}} = \boldsymbol{R}\tilde{\boldsymbol{\Lambda}}_1 + \tilde{\boldsymbol{E}}_1 \tag{28}$$

$$\hat{\boldsymbol{A}} = \boldsymbol{A}\tilde{\boldsymbol{\Lambda}}_2 + \tilde{\boldsymbol{E}}_2 \tag{29}$$

$$\hat{\boldsymbol{B}} = \boldsymbol{A}^*\tilde{\boldsymbol{\Lambda}}_3 + \tilde{\boldsymbol{E}}_3 \tag{30}$$

where $\tilde{\boldsymbol{\Lambda}}_1, \tilde{\boldsymbol{\Lambda}}_2, \tilde{\boldsymbol{\Lambda}}_3$ are unknown nonsingular diagonal matrices with their diagonal elements lying on the unit circle.

Notice that the kth column of $\boldsymbol{A}$ is characterized by the DoA and carrier frequency associated with the kth source. We now discuss how to estimate $\{\omega_k\}$ and $\{\tau_k\}$ from the estimated factor matrix $\hat{\boldsymbol{A}}$. Note that $\hat{\boldsymbol{B}}$ is also an estimate of $\boldsymbol{A}$. Therefore either $\hat{\boldsymbol{A}}$ or $\hat{\boldsymbol{B}}$ can be used to estimate $\{\omega_k\}$ and $\{\tau_k\}$. Let $\hat{\boldsymbol{a}}_k$ denote the k-th column of $\hat{\boldsymbol{A}}$, and write

$$\tilde{\boldsymbol{\Lambda}}_2 = \mathrm{diag}\{e^{-j\varphi_1}, \ldots, e^{-j\varphi_K}\} \tag{31}$$

where $\{\varphi_k\} \in [0, 2\pi)$ are unknown parameters. To simplify our exposition, we ignore the estimation errors $\tilde{\boldsymbol{E}}_1$, $\tilde{\boldsymbol{E}}_2$, and $\tilde{\boldsymbol{E}}_3$.

Write $z = re^{j\varphi}$, and define $\arg(z) \triangleq \mathrm{mod}(\varphi, 2\pi)$ where $\mathrm{mod}(a, b)$ is a modulo operator which returns the remainder of the Euclidean division of a by b. Recalling (13), we have

$$\begin{aligned}\eta_{nk} &\triangleq \mathrm{mod}\left(-\arg(\hat{a}_{nk}), 2\pi\right) \\ &= \mathrm{mod}\left((n-1)\tau_k\omega_k + \Delta_n\omega_k + \varphi_k, 2\pi\right)\end{aligned} \tag{32}$$

where $\hat{a}_{nk}$ denotes the nth entry of $\hat{\boldsymbol{a}}_k$. Let $\boldsymbol{\eta}_k \triangleq [\eta_{1k} \ \ldots \ \eta_{Nk}]^T$ and let $\boldsymbol{D}_p$ denote a difference matrix defined as

$$\boldsymbol{D}_p \triangleq \begin{pmatrix} -1 & 1 & 0 & \ldots & 0 \\ 0 & -1 & 1 & \ldots & 0 \\ \vdots & \vdots & \ddots & \ddots & \vdots \\ 0 & 0 & \ldots & -1 & 1 \end{pmatrix} \in \mathbb{R}^{(p-1)\times p}$$

To recover ω_k, we conduct a two-stage difference operation as follows

$$\boldsymbol{\beta}_k^{(1)} = \mathrm{mod}(\boldsymbol{D}_N\boldsymbol{\eta}_k, 2\pi) \tag{33}$$

$$\boldsymbol{\beta}_k^{(2)} = \mathrm{mod}(\boldsymbol{D}_{N-1}\boldsymbol{\beta}_k^{(1)}, 2\pi) \tag{34}$$

It can be easily verified that entries of $\boldsymbol{\beta}_k^{(1)}$ and $\boldsymbol{\beta}_k^{(2)}$ are respectively given as

$$\beta_{nk}^{(1)} = \mathrm{mod}\left(\tau_k\omega_k + (\Delta_{n+1} - \Delta_n)\omega_k, 2\pi\right), \quad n = 1, \ldots, N-1 \tag{35}$$

$$\beta_{nk}^{(2)} = \mathrm{mod}\left((\Delta_{n+2} - 2\Delta_{n+1} + \Delta_n)\omega_k, 2\pi\right), \quad n = 1, \ldots, N-2 \tag{36}$$

From (36), we can see that the information about the carrier frequency ω_k is extracted after performing the two-stage difference operation. By properly devising the time delay factors $\{\Delta_n\}$, we can ensure that for some $n_0 \in \{1, \ldots, N-2\}$, the condition (5) holds valid, i.e.

$$0 < (\Delta_{n_0+2} - 2\Delta_{n_0+1} + \Delta_{n_0})f_{\text{nyq}} \leq 1 \tag{37}$$

The above condition implies

$$0 < (\Delta_{n_0+2} - 2\Delta_{n_0+1} + \Delta_{n_0})\omega_{\max} \leq 2\pi \tag{38}$$

where $\omega_{\max} \triangleq \max\{\omega_1, \ldots, \omega_K\}$. Therefore ω_k can simply be estimated as

$$\hat{\omega}_k = \frac{\beta_{n_0,k}^{(2)}}{\Delta_{n_0+2} - 2\Delta_{n_0+1} + \Delta_{n_0}} \tag{39}$$

In fact, for a careful selection of time delay factors $\{\Delta_n\}$, the condition (5) (i.e. (37)) may be satisfied for different choices of n. As a result, we can obtain multiple estimates of $\hat{\omega}_k$. To improve the estimation performance, a final estimate of $\hat{\omega}_k$ can be chosen as the average of these multiple estimates. We emphasize that the average operation is not necessarily needed by our proposed algorithm. It is just an option which we can use

to enhance the estimation accuracy. In other words, as long as (37) holds valid for some $n_0 \in \{1, \ldots, N-2\}$, perfect recovery of the carrier frequency is guaranteed if noise and sample covariance estimation errors are ignored.

Under Assumption A7, that is, $d < C/(2f_{\text{nyq}})$, we have $|\tau_k \omega_{\max}| < \pi$. Thus, substituting the estimated $\hat{\omega}_k$ back into (35), τ_k can be obtained as

$$\hat{\tau}_k = \frac{\text{mod}\left(\beta_{nk}^{(1)} - (\Delta_{n+1} - \Delta_n)\hat{\omega}_k + \pi, 2\pi\right) - \pi}{\hat{\omega}_k} \tag{40}$$

Note that for each $\beta_{nk}^{(1)}, n = 1, \ldots, N-1$, we can obtain an estimate of τ_k. Therefore multiple estimates of τ_k can be collected. Again, an average operation can be conducted to yield a final estimate of τ_k. Based on $\hat{\tau}_k$, an estimate of the associated DoA θ_k can be readily obtained from (8).

We now discuss how to recover the power spectra of the sources $\{s_k(t)\}$. Let $\tilde{r}_k^s(\tau) \triangleq R_k^s(t+\tau, t)$, where $\tau \in \mathbb{R}$ can be any real value. The power spectrum of the kth source can thus be expressed as the Fourier transform of $\tilde{r}_k^s(\tau)$, i.e.

$$\tilde{S}_k(\omega) = \int_{-\infty}^{+\infty} \tilde{r}_k^s(\tau) e^{-j\omega\tau} \mathrm{d}\tau \tag{41}$$

Let $S_k(\omega)$ denote the discrete-time Fourier transform (DTFT) of the autocorrelation sequence $\{r_k^s(l)\}_{l=-\infty}^{+\infty}$, i.e.

$$S_k(\omega) = \sum_{l=-\infty}^{\infty} r_k^s(l) e^{-j\omega l T_s} \tag{42}$$

According to the sampling theorem, $\tilde{S}_k(\omega)$ and $S_k(\omega)$ are related as follows

$$S_k(\omega) = \frac{1}{T_s} \sum_{n=-\infty}^{+\infty} \tilde{S}_k\left(\omega + n\frac{2\pi}{T_s}\right) \tag{43}$$

Under Assumption A6, i.e. $f_s \geq B \geq B_k$, the power spectrum $\tilde{S}_k(\omega)$ can be perfectly recovered by filtering $S_k(\omega)$ with a bandpass filter, i.e.

$$\tilde{S}_k(\omega) = \begin{cases} T_s S_k(\omega), & \omega \in [\omega_k - \pi f_s, \omega_k + \pi f_s] \\ 0, & \omega \notin [\omega_k - \pi f_s, \omega_k + \pi f_s] \end{cases}. \tag{44}$$

Given the estimated factor matrix $\hat{\boldsymbol{R}}$, the DTFT of the autocorrelation sequence $\{r_k^s(l)\}$ can be approximated as

$$\hat{S}_k(\omega) = \sum_{l=-L}^{L} \hat{r}_k^s(l) e^{-j\omega l T_s} \tag{45}$$

When L is chosen to be sufficiently large, the estimation error due to the time lag truncation is negligible. Also, although there exists a phase ambiguity between the estimated autocorrelation sequence $\hat{\boldsymbol{r}}_k$ and the true autocorrelation sequence $\boldsymbol{r}_k$, this phase ambiguity can be removed by noting that the power spectrum $S_k(\omega)$ is real and non-negative. In addition, the power spectrum of each source is automatically paired with its associated DoA and carrier frequency due to the reason that both $\hat{\boldsymbol{R}}$ and $\hat{\boldsymbol{A}}$ experience a common permutation operation.

C. Uniqueness of CP Decomposition

We see that the uniqueness of the CP decomposition is crucial to our proposed method. It is well known that the essential uniqueness of CP decomposition can be guaranteed by Kruskal's condition [29]. Let $k_{\boldsymbol{X}}$ denote the k-rank of a matrix $\boldsymbol{X}$, which is defined as the largest value of $k_{\boldsymbol{X}}$ such that every subset of $k_{\boldsymbol{X}}$ columns of the matrix $\boldsymbol{X}$ is linearly independent. We have the following theorem concerning the uniqueness of CP decomposition.

Theorem 1: Let $(\boldsymbol{X}, \boldsymbol{Y}, \boldsymbol{Z})$ be a CP solution which decomposes a third-order tensor $\boldsymbol{\mathcal{X}} \in \mathbb{C}^{d_1 \times d_2 \times d_3}$ into p rank-one arrays, where $\boldsymbol{X} \in \mathbb{C}^{d_1 \times p}$, $\boldsymbol{Y} \in \mathbb{C}^{d_2 \times p}$, and $\boldsymbol{Z} \in \mathbb{C}^{d_3 \times p}$. Suppose the following Kruskal's condition

$$k_{\boldsymbol{X}} + k_{\boldsymbol{Y}} + k_{\boldsymbol{Z}} \geq 2p + 2 \tag{46}$$

holds and there is an alternative CP solution $(\hat{\boldsymbol{X}}, \hat{\boldsymbol{Y}}, \hat{\boldsymbol{Z}})$ which also decomposes $\boldsymbol{\mathcal{X}}$ into p rank-one arrays. Then we have $\hat{\boldsymbol{X}} = \boldsymbol{X}\boldsymbol{\Pi}\boldsymbol{\Lambda}_x$, $\hat{\boldsymbol{Y}} = \boldsymbol{Y}\boldsymbol{\Pi}\boldsymbol{\Lambda}_y$, and $\hat{\boldsymbol{Z}} = \boldsymbol{Z}\boldsymbol{\Pi}\boldsymbol{\Lambda}_z$, where $\boldsymbol{\Pi}$ is a unique permutation matrix and $\boldsymbol{\Lambda}_x$, $\boldsymbol{\Lambda}_y$, and $\boldsymbol{\Lambda}_z$ are unique diagonal matrices such that $\boldsymbol{\Lambda}_x\boldsymbol{\Lambda}_y\boldsymbol{\Lambda}_z = \boldsymbol{I}$.

Proof: A rigorous proof can be found in [30]. ■

Note that Kruskal's condition cannot hold when $R = 1$. However, in that case the uniqueness has been proven by Harshman [31]. Kruskal's sufficient condition is also necessary for $R = 2$ and $R = 3$, but not for $R > 3$ [30].

From the above theorem, we know that if

$$k_{\boldsymbol{R}} + k_{\boldsymbol{A}} + k_{\boldsymbol{A}^*} \geq 2K + 2 \tag{47}$$

then the CP decomposition of $\boldsymbol{\mathcal{R}}^x$ is essentially unique. Since $\boldsymbol{A}^*$ is the complex conjugate of $\boldsymbol{A}$, we only need to examine the k-ranks of $\boldsymbol{A}$ and $\boldsymbol{R}$.

Note that the (n,k)th entry of $\boldsymbol{A}$ is given by $a_{nk} = e^{-j((n-1)\tau_k\omega_k + \Delta_n\omega_k)}$, which is a function of the time delay factor Δ_n. It is not difficult to design a set of time delay factors $\{\Delta_n\}$ such that $k_{\boldsymbol{A}} = K$. For example, we divide N antennas into two groups $S_1 = \{1, \ldots, K\}$ and $S_2 = \{K+1, \ldots, N\}$. We set the delay factors in the first group to be linearly proportional to $n-1$, i.e. $\Delta_n = (n-1)\nu$ for $n \in S_1$, where $\nu \geq 0$ is a constant. In this case, the first K rows of $\boldsymbol{A}$ form a Vandermonde matrix:

$$\boldsymbol{A}_{[1:K,:]} = \text{Vand}(\tau_1\omega_1 + \nu\omega_1, \ldots, \tau_K\omega_K + \nu\omega_K) \tag{48}$$

where $\text{Vand}(\phi_1, \ldots, \phi_K)$ is defined as

$$\text{Vand}(\phi_1, \ldots, \phi_K) \triangleq \begin{bmatrix} e^{-j(0\phi_1)} & \cdots & e^{-j(0\phi_K)} \\ e^{-j(1\phi_1)} & \cdots & e^{-j(1\phi_K)} \\ \vdots & \ddots & \vdots \\ e^{-j((K-1)\phi_1)} & \cdots & e^{-j((K-1)\phi_K)} \end{bmatrix}$$

Thus $\boldsymbol{A}$ is full column rank with $k_{\boldsymbol{A}} = K$ as long as $\{\omega_k\tau_k + \nu\omega_k\}$ are distinct from each other. If we set $\nu = 0$, we only need $\{\omega_k\tau_k\}$, i.e. $\{\omega_k \cos\theta_k\}$, are distinct from each other. For the case where the quantities $\{\omega_k \cos\theta_k\}$ for different source signals may be identical, we can set $\nu \neq 0$, in which case we still have $k_{\boldsymbol{A}} = K$ provided that the carrier frequencies $\{\omega_k\}$ are mutually different. In other words, as long as Assumption A4

is satisfied, we can always set an appropriate value of ν to ensure $k_{\boldsymbol{A}} = K$. For other more general choices of time delay factors $\{\Delta_n\}$, it can be numerically checked that the k-rank of $\boldsymbol{A}$ still equals to K with a high probability, although a rigorous proof is difficult.

Since we have $k_{\boldsymbol{A}} = K$, we only need $k_{\boldsymbol{R}} \geq 2$ in order to satisfy Kruskal's condition. This condition $k_{\boldsymbol{R}} \geq 2$ is met if every two columns of $\boldsymbol{R}$ are linearly independent. Note that the kth column of $\boldsymbol{R}$, $\boldsymbol{r}_k$, is a truncated autocorrelation sequence of the kth modulated signal $s_k(t)e^{j\omega_k t}$. Clearly, if the baseband signals $\{s_k(t)\}$ have distinct power spectra, then any two columns of $\boldsymbol{R}$ are linearly independent, which implies $k_{\boldsymbol{R}} \geq 2$. In practice, since source signals usually have different bandwidths, the diverse power spectra condition can be easily satisfied. Even if the baseband signals $\{s_k(t)\}$ have identical power spectra, the autocorrelation sequences of any two modulated signals $\{s_{k_1}(t)e^{j\omega_{k_1} t}, s_{k_2}(t)e^{j\omega_{k_2} t}\}$ could still be linearly independent as long as their carrier frequencies satisfy

$$\operatorname{mod}\{|\omega_{k_1} - \omega_{k_2}|, 2\pi f_s\} \neq 0 \tag{49}$$

The above condition ensures that autocorrelation sequences $\{\boldsymbol{r}_k\}$ of different modulated signals have distinct exponential terms $\{e^{j\omega_k l T_s}\}$ (see (12)). Due to the randomness of locations of the carrier frequencies, the condition (49) is very likely to be satisfied in practice. As a result, we have $k_{\boldsymbol{R}} \geq 2$.

VI. Discussions and Extensions

A. Exact Recovery Condition

Here we provide a brief review and discussion of exact recovery conditions for our proposed method. In fact, most of these conditions have been summarized as basic assumptions listed in Section III and Section IV.

First of all, for our proposed method, the number of antennas is assumed to be greater than the number of source signals, i.e. $N > K$. This condition implies that a minimum number of antennas needed for our proposed algorithm is $K + 1$. On the other hand, our proposed method requires the minimum sampling rate per channel satisfies $f_s \geq B$. Therefore the overall sampling rate, f_{os}, defined as the total number of sampling channels times the sampling rate per channel, should be no smaller than

$$f_{os} \geq (K + 1)B \tag{50}$$

This overall sampling rate condition (50) is less restrictive than that of existing works, such as [18], [20]. Specifically, the work [18] needs to satisfy $f_{os} \geq (2K + 2)B$ because its number of sampling channels is twice the number of antennas N and N has to be greater than K, i.e. $N \geq K + 1$. For the work [20], its number of sampling channels is identical to the number of antennas which is no less than $2K + 1$. Thus its overall sampling rate has to satisfy $f_{os} \geq (2K + 1)B$. We see that the overall sampling rate required by our proposed method for perfect signal/parameter recovery is about half of that required by [18], [20]. Another point we would like to clarify is that our proposed method does not need to impose a sparsity constraint on the frequency domain. In fact, our proposed method allows for perfect recovery even when the frequency domain is crowded with signals. Moreover, our proposed algorithm is capable of separating narrowband signals with partially overlapping frequency bands, as will be corroborated by our simulation results.

Another important characteristic of our proposed method is its ability to accommodate flexible time delays. As discussed earlier, the time delay factors can take arbitrary values as long as Assumption A5 is satisfied. Although the uniqueness of CP decomposition also involves design of time delay factors, as analyzed in the previous section, for general choices of time delay factors, we usually have $k_{\boldsymbol{A}} = K$ such that the uniqueness of CP decomposition can be guaranteed.

B. Extension to Array With Other Geometries

Our proposed algorithm is not only applicable to uniform linear arrays, but can also be extended to arrays with other geometries such as sparse arrays. Details of this extension are discussed below.

Let $\{c_1, c_2, \ldots, c_M\} \subset \{1, \ldots, N\}$ denote the indices of antennas which are selected from a uniform linear array, where $1 \leq c_1 < c_2 < \cdots < c_M \leq N$ and $M > K$. Following the approach in Section V, we construct a third-order tensor $\boldsymbol{\mathcal{R}}^x \in \mathbb{C}^{(2L-1)\times M\times M}$, with its (l, m, n)-th entry given by $r^x_{c_m, c_n}(l)$. Similar to (17), the tensor $\boldsymbol{\mathcal{R}}^x$ can be expressed as

$$\boldsymbol{\mathcal{R}}^x = \sum_{k=1}^{K} \boldsymbol{r}_k \circ \bar{\boldsymbol{a}}_k \circ \bar{\boldsymbol{a}}_k^* + \boldsymbol{\mathcal{R}}^w \tag{51}$$

where $\boldsymbol{\mathcal{R}}^w \in \mathbb{C}^{(2L-1)\times M\times M}$ is a third-order tensor with its (l, m, n)-th entry given by $r^w_{c_m, c_n}(l)$ and $\bar{\boldsymbol{a}}_k \triangleq [a_{c_1 k} \;\; a_{c_2 k} \;\; \ldots \;\; a_{c_M k}]^T$. Define $\bar{\boldsymbol{A}} \triangleq [\bar{\boldsymbol{a}}_1 \; \ldots \; \bar{\boldsymbol{a}}_K]$. The three matrices $\{\boldsymbol{R}, \bar{\boldsymbol{A}}, \bar{\boldsymbol{A}}^*\}$ are factor matrices associated with the noiseless version of $\boldsymbol{\mathcal{R}}^x$.

Next, we discuss how to estimate carrier frequencies and DoAs from the factor matrix $\hat{\bar{\boldsymbol{A}}}$ estimated from the CP decomposition. Since the columns of $\bar{\boldsymbol{A}}/\sqrt{M}$ have unit norm, the amplitude ambiguity can be estimated and removed. By ignoring the estimation errors, $\hat{\bar{\boldsymbol{A}}}$ and $\bar{\boldsymbol{A}}$ are related as $\hat{\bar{\boldsymbol{A}}} = \bar{\boldsymbol{A}}\boldsymbol{\Lambda}$, where $\boldsymbol{\Lambda}$ is an unknown nonsingular diagonal matrix with its diagonal elements $\{e^{-j\varphi_k}\}$ lying on the unit circle. Let $\hat{\bar{\boldsymbol{a}}}_k$ denote the kth column of $\hat{\bar{\boldsymbol{A}}}$. We have

$$\begin{aligned}\bar{\eta}_{m k} &\triangleq \operatorname{mod}(-\arg(\hat{a}_{c_m k}), 2\pi) \\ &= \operatorname{mod}((c_m - 1)\tau_k\omega_k + \Delta_{c_m}\omega_k + \varphi_k, 2\pi)\end{aligned} \tag{52}$$

where $\hat{a}_{c_m k}$ denotes the mth entry of $\hat{\bar{\boldsymbol{a}}}_k$. Let $\bar{\boldsymbol{\eta}}_k \triangleq [\bar{\eta}_{c_1 k} \;\; \ldots \;\; \bar{\eta}_{c_M k}]^T$. Again, a two-stage difference operation is performed to recover ω_k and θ_k:

$$\bar{\boldsymbol{\beta}}_k^{(1)} = \operatorname{mod}(\boldsymbol{D}_M \bar{\boldsymbol{\eta}}_k, 2\pi) \tag{53}$$

$$\bar{\boldsymbol{\beta}}_k^{(2)} = \operatorname{mod}(\boldsymbol{D}_{M-1} \bar{\boldsymbol{\beta}}_k^{(1)}, 2\pi) \tag{54}$$

It can be easily verified that entries of $\bar{\boldsymbol{\beta}}_k^{(1)}$ and $\bar{\boldsymbol{\beta}}_k^{(2)}$ are respectively given as

$$\begin{aligned}\bar{\beta}_{mk}^{(1)} &= \mathrm{mod}\big((c_{m+1}-c_m)\tau_k\omega_k \\ &\qquad + (\Delta_{c_{m+1}}-\Delta_{c_m})\omega_k, 2\pi\big), \\ m &= 1,\ldots,M-1 \end{aligned} \tag{55}$$

$$\begin{aligned}\bar{\beta}_{mk}^{(2)} &= \mathrm{mod}\big((c_{m+2}-2c_{m+1}+c_m)\tau_k\omega_k \\ &\qquad + (\Delta_{c_{m+2}}-2\Delta_{c_{m+1}}+\Delta_{c_m})\omega_k, 2\pi\big), \\ m &= 1,\ldots,M-2 \end{aligned} \tag{56}$$

Clearly, if there exists an $m_1 \in \{1,\ldots,M-2\}$ which satisfies

$$c_{m_1+2} - 2c_{m_1+1} + c_{m_1} = 0 \tag{57}$$

and

$$0 < (\Delta_{c_{m_1+2}} - 2\Delta_{c_{m_1+1}} + \Delta_{c_{m_1}}) f_{\text{nyq}} \le 1 \tag{58}$$

then ω_k can be perfectly extracted from (56). Substituting the estimated $\hat{\omega}_k$ back into (55), τ_k (i.e. θ_k) can be recovered from (55) if there exists an $m_2 \in \{1,\ldots,M-1\}$ which satisfies

$$c_{m_2+1} - c_{m_2} = 1 \tag{59}$$

From the above discussion, we see that our proposed algorithm can be easily adapted to sparse arrays, provided that the index set $\{c_1, c_2, \ldots, c_M\}$ is properly chosen to satisfy (57) and (59) for a certain $m_1 \in \{1,\ldots,M-2\}$ and $m_2 \in \{1,\ldots,M-1\}$. Also, it should be noted that the condition (5) placed on time delay factors is now replaced by (58).

Lastly, we would like to emphasize that the problem considered in our paper is very different from the problem considered in some sparse-array related works, e.g. [32]–[34]. In these works [32]–[34], the carrier frequency of source signals is assumed to be the same and known *a priori*, and the problem of interest is to estimate the DoAs associated with different signals. Thus, sub-Nyquist sampling is not necessarily needed in these works. In fact, these works are mainly concerned about spatial compression and the design of the spatial sampling pattern to improve the degree of freedom for array signal processing. In contrast, our work considers the problem of joint spectrum sensing and DoA estimation, in which the source signals spread over a wide frequency band and the carrier frequencies of the source signals are unknown *a priori*. To overcome the sampling rate bottleneck for wideband spectrum sensing, a sub-Nyquist sampling architecture has to be employed.

VII. CRB Analysis

In this section, we develop Cramér-Rao bound (CRB) results for the joint DoA, carrier frequency, and power spectra estimation problem considered in this paper. As is well known, the CRB is a lower bound on the variance of any unbiased estimator [35]. It provides a benchmark for evaluating the performance of our proposed method. In addition, the CRB results illustrate the behavior of the resulting bounds, which helps understand the effect of different system parameters, including the noise power σ^2, the number of antennas N and the number of samples N_s, on the estimation performance.

A. Signal Model

Recall that the analog signal at each antenna is sampled with a sampling rate $f_s = 1/T_s$. The sampled signal at the nth antenna can be written as (cf. (7))

$$x_n(lT_s) = \sum_{k=1}^{K} a_{nk}\, s_k(lT_s) e^{j\omega_k (lT_s)} + w_n(lT_s) \tag{60}$$

The above signal model can be rewritten in a vector-matrix form as

$$\boldsymbol{x}_l = \boldsymbol{A}\boldsymbol{s}_l + \boldsymbol{w}_l, \quad l = 0,\ldots,N_s-1 \tag{61}$$

where $\boldsymbol{A}$ is defined in (18), $\boldsymbol{x}_l \triangleq [x_1(lT_s) \ \ldots \ x_N(lT_s)]^T$, $\boldsymbol{w}_l \triangleq [w_1(lT_s) \ \ldots \ w_N(lT_s)]^T$ and

$$\boldsymbol{s}_l \triangleq \Big[s_1(lT_s)e^{j\omega_1(lT_s)} \ \ldots \ s_K(lT_s)e^{j\omega_K(lT_s)}\Big]^T$$

Suppose we collect a total number of N_s ($l = 0,\ldots,N_s-1$) samples. The received signal can thus be expressed as

$$\boldsymbol{X} = \boldsymbol{A}\boldsymbol{S} + \boldsymbol{W} \tag{62}$$

where $\boldsymbol{X} \triangleq [\boldsymbol{x}_0 \ \ldots \ \boldsymbol{x}_{N_s-1}]$, $\boldsymbol{S} \triangleq [\boldsymbol{s}_0 \ \ldots \ \boldsymbol{s}_{N_s-1}]$ and $\boldsymbol{W} \triangleq [\boldsymbol{w}_0 \ \ldots \ \boldsymbol{w}_{N_s-1}]$. Let $\boldsymbol{x} \triangleq \mathrm{vec}(\boldsymbol{X}^T)$, where $\mathrm{vec}(\boldsymbol{Z})$ denotes a vectorization operation which stacks the columns of $\boldsymbol{Z}$ into a single column vector. We have

$$\boldsymbol{x} = \tilde{\boldsymbol{A}}\boldsymbol{s} + \boldsymbol{w} \tag{63}$$

where $\boldsymbol{x} \triangleq \mathrm{vec}(\boldsymbol{X}^T)$, $\boldsymbol{w} \triangleq \mathrm{vec}(\boldsymbol{W}^T)$, $\boldsymbol{s} \triangleq \mathrm{vec}(\boldsymbol{S}^T)$ and

$$\tilde{\boldsymbol{A}} \triangleq \boldsymbol{A} \otimes \boldsymbol{I}_{N_s} \tag{64}$$

in which $\boldsymbol{I}_n$ denotes an $n \times n$ identity matrix. We assume that $\boldsymbol{w} \sim \mathcal{CN}(\boldsymbol{0}, \sigma^2 \boldsymbol{I}_{N\cdot N_s})$ and $\boldsymbol{s} \sim \mathcal{CN}(\boldsymbol{0}, \boldsymbol{R}_s)$ follow a circularly-symmetric complex Gaussian distribution, where $\boldsymbol{R}_s$ denotes the source covariance matrix which needs to be estimated along with other parameters. Note that in our proposed algorithm, the additive noise $\boldsymbol{w}$ and the source signal $\boldsymbol{s}$ are not restricted to be circularly-symmetric complex Gaussian. Here we make such an assumption in order to facilitate the CRB analysis.

Under the assumption that $\boldsymbol{w}$ and $\boldsymbol{s}$ are circularly-symmetric complex Gaussian random variables, we can readily verify that $\boldsymbol{x}$ also follows a circularly-symmetric complex Gaussian distribution, i.e. $\boldsymbol{x} \sim \mathcal{CN}(\boldsymbol{0}, \boldsymbol{R}_x)$, where

$$\boldsymbol{R}_x \triangleq \mathbb{E}\left[\boldsymbol{x}\boldsymbol{x}^H\right] = \tilde{\boldsymbol{A}}\boldsymbol{R}_s\tilde{\boldsymbol{A}}^H + \sigma^2\boldsymbol{I}_{NN_s} \tag{65}$$

From Assumption A2, we know that $\boldsymbol{R}_s$ is a block diagonal matrix, i.e.

$$\boldsymbol{R}_s = \mathrm{diag}(\boldsymbol{P}_1,\ldots,\boldsymbol{P}_K). \tag{66}$$

where $\boldsymbol{P}_k \triangleq \mathbb{E}[\tilde{\boldsymbol{s}}_k\tilde{\boldsymbol{s}}_k^H]$ denotes the autocorrelation matrix of the kth signal, and $\tilde{\boldsymbol{s}}_k$ is the transpose of the kth row of $\boldsymbol{S}$, i.e. $\tilde{\boldsymbol{s}}_k \triangleq [s_k(0T_s)e^{j\omega_k(0T_s)} \ldots s_k((N_s-1)T_s)e^{j\omega_k((N_s-1)T_s)}]^T$. Also, in Assumption A2, each source is assumed to be wide-sense stationary. Therefore the autocorrelation matrix $\boldsymbol{P}_k$ is a Hermitian-Toeplitz matrix. Here Toeplitz means that it has diagonal-constant entries, i.e. each descending diagonal from left to right is constant. Let p_0^k denote the constant for elements located on

the main diagonal, and p_l^k, $l \geq 1$, denote the constant for elements located on the lth diagonal below the main diagonal of $\boldsymbol{P}_k$. Let

$$\boldsymbol{T}_l \triangleq \begin{pmatrix} \boldsymbol{0} & \boldsymbol{I}_{N_s-l} \\ \boldsymbol{0} & \boldsymbol{0} \end{pmatrix} \in \mathbb{R}^{N_s \times N_s}$$

and $\boldsymbol{T}_{-l} \triangleq \boldsymbol{T}_l^T$. The autocorrelation matrix $\boldsymbol{P}_k$ can thus be expressed as

$$\boldsymbol{P}_k = p_0^k \boldsymbol{I}_{N_s} + \sum_{l=1}^{L} \left[p_l^k \boldsymbol{T}_{-l} + (p_l^k)^* \boldsymbol{T}_l \right] \tag{67}$$

where L is chosen to be sufficiently large to ensure $p_l^k = 0$ for $l > L$. From (67), we can see that $\boldsymbol{P}_k$ is characterized by parameters

$$\boldsymbol{p}_k \triangleq \left[p_0^k \;\; \Re(p_1^k) \;\; \ldots \;\; \Re(p_L^k) \;\; \Im(p_1^k) \;\; \ldots \;\; \Im(p_L^k) \right] \tag{68}$$

As a result, $\boldsymbol{R}_s$ is characterized by parameters

$$\boldsymbol{p} \triangleq [\boldsymbol{p}_1 \;\; \ldots \;\; \boldsymbol{p}_K] \tag{69}$$

On the other hand, notice that $\boldsymbol{A}$ is a parameterized matrix, with each column of $\boldsymbol{A}$ determined by the DoA and the carrier frequency of each source, i.e. $\{\theta_k, \omega_k\}$. Unfortunately, the value ranges for the DoA and the carrier frequency differ by orders of magnitude, which may cause numerical instability in computing the CRB matrix. To address this difficulty, we, instead, analyze the CRB for the following two parameters $\{\xi_k, \psi_k\}$ defined as

$$\xi_k \triangleq \omega_k \tau_k, \qquad \psi_k \triangleq \omega_k / c \tag{70}$$

where c is a parameter appropriate chosen (e.g. $c = 10^9$) such that values of ξ_k and ψ_k roughly have the same scale. Also, we define $\boldsymbol{\xi} \triangleq [\xi_1 \;\; \ldots \;\; \xi_K]$ and $\boldsymbol{\psi} \triangleq [\psi_1 \;\; \ldots \;\; \psi_K]$.

We see that the complete set of parameters to be estimated include

$$\boldsymbol{\alpha} \triangleq \left[\boldsymbol{\xi} \;\; \boldsymbol{\psi} \;\; \boldsymbol{p} \;\; \sigma^2 \right] \tag{71}$$

Recall that $\boldsymbol{x}$ follows a complex Gaussian distribution with zero mean and covariance matrix $\boldsymbol{R}_x$. Therefore the log-likelihood function of $\boldsymbol{\alpha}$ can be expressed as

$$L(\boldsymbol{\alpha}) \propto -\ln |\boldsymbol{R}_x| - \boldsymbol{x}^H \boldsymbol{R}_x^{-1} \boldsymbol{x} \tag{72}$$

B. Calculation of the CRB Matrix

Since the random vector $\boldsymbol{x}$ follows a circularly-symmetric complex Gaussian distribution, we can resort to the Slepian-Bangs formula [36], [37] to compute the Fisher information matrix (FIM). According to the Slepian-Bangs formula, the (i, j)th element of the FIM $\boldsymbol{\Omega}$ is calculated as

$$\Omega_{ij} = \mathrm{tr}\left(\boldsymbol{R}_x^{-1} \frac{\partial \boldsymbol{R}_x}{\partial \alpha_i} \boldsymbol{R}_x^{-1} \frac{\partial \boldsymbol{R}_x}{\partial \alpha_j} \right) \tag{73}$$

where α_i and α_j denote the ith and the jth entries of $\boldsymbol{\alpha}$, respectively.

By utilizing the structures of $\tilde{\boldsymbol{A}}$ and $\boldsymbol{R}_s$ (cf. (64) and (66)), $\boldsymbol{R}_x$ can be expressed as

$$\boldsymbol{R}_x = \sum_{k=1}^{K} (\boldsymbol{a}_k \boldsymbol{a}_k^H) \otimes \boldsymbol{P}_k + \sigma^2 \boldsymbol{I}_{N \cdot N_s} \tag{74}$$

where $\boldsymbol{a}_k$, defined in (16), is the kth column of $\boldsymbol{A}$.

We first compute the partial derivative of $\boldsymbol{R}_x$ with respect to ξ_k and ψ_k. From (13) and the definition of $\{\xi_k, \psi_k\}$, we can write $a_{nk} = e^{-j((n-1)\xi_k + c\Delta_n \psi_k)}$. Thus we have

$$\partial \boldsymbol{a}_k / \partial \xi_k = -j \cdot \mathrm{diag}(0, \ldots, N-1) \cdot \boldsymbol{a}_k \tag{75}$$

$$\partial \boldsymbol{a}_k / \partial \psi_k = -j \cdot c \cdot \mathrm{diag}(\Delta_1, \ldots, \Delta_N) \cdot \boldsymbol{a}_k \tag{76}$$

Combining (74) and (75)–(76), we have

$$\partial \boldsymbol{R}_x / \partial \xi_k = \left((\partial \boldsymbol{a}_k / \partial \xi_k) \boldsymbol{a}_k^H + \boldsymbol{a}_k (\partial \boldsymbol{a}_k^H / \partial \xi_k) \right) \otimes \boldsymbol{P}_k \tag{77}$$

$$\partial \boldsymbol{R}_x / \partial \psi_k = \left((\partial \boldsymbol{a}_k / \partial \psi_k) \boldsymbol{a}_k^H + \boldsymbol{a}_k (\partial \boldsymbol{a}_k^H / \partial \psi_k) \right) \otimes \boldsymbol{P}_k \tag{78}$$

Similarly, we can obtain the partial derivatives with respect to other parameters as follows

$$\partial \boldsymbol{R}_x / \partial (p_0^k) = \left(\boldsymbol{a}_k \boldsymbol{a}_k^H \right) \otimes \boldsymbol{I}_{N_s} \tag{79}$$

$$\partial \boldsymbol{R}_x / \partial (\Re(p_l^k)) = \left(\boldsymbol{a}_k \boldsymbol{a}_k^H \right) \otimes (\boldsymbol{T}_{-l} + \boldsymbol{T}_l) \tag{80}$$

$$\partial \boldsymbol{R}_x / \partial (\Im(p_l^k)) = \left(\boldsymbol{a}_k \boldsymbol{a}_k^H \right) \otimes (j\boldsymbol{T}_{-l} - j\boldsymbol{T}_l) \tag{81}$$

and

$$\partial \boldsymbol{R}_x / \partial (\sigma^2) = \boldsymbol{I}_{N \cdot N_s}. \tag{82}$$

After obtaining the FIM $\boldsymbol{\Omega}$, the CRB can be calculated as [35]

$$\mathrm{CRB}(\boldsymbol{\alpha}) = \boldsymbol{\Omega}^{-1}. \tag{83}$$

VIII. Simulation Results

In this section, we carry out experiments to illustrate the performance of our proposed method. In our simulations, we set $f_{\mathrm{nyq}} = 1$ GHz. The distance between two adjacent antennas, d, is set equal to $d = 0.4 \times C / f_{\mathrm{nyq}}$ in order to meet the condition in Assumption A7. The number of antennas is set to $N = 8$, and for simplicity, the time delay factors are set as

$$\Delta_n = \begin{cases} 0 \text{ s}, & n = 1, \ldots, N/2 \\ 10^{-9} \text{ s}, & n = N/2+1, \ldots, N \end{cases} \tag{84}$$

With this setup, the condition (5) can be satisfied for $n = N/2 - 1$. The signal-to-noise ratio (SNR) is defined as $\mathrm{SNR} \triangleq \mathbb{E}[|s(t)|^2]/\sigma^2$.

We first consider the case in which $K = 3$ uncorrelated, wide-sense stationary sources spreading over the wide frequency band (0, 1] GHz impinge on a ULA of N antennas. The DoAs of these three sources are given respectively by $\theta_1 = 2.051$, $\theta_2 = 1.447$, and $\theta_3 = 0.361$. The carrier frequencies and bandwidths associated with these sources are set to $f_1 = 152$ MHz, $f_2 = 323$ MHz, $f_3 = 432$ MHz, $B_1 = 20$ MHz, $B_2 = 20$ MHz, and $B_3 = 15$ MHz. The complex baseband signals are generated by passing the complex white Gaussian noise through low-pass filters with different cutoff frequencies. Also, the number of data samples used for calculating the correlation matrices is set to $N_s = 10^5$. The sampling rate f_s is chosen to be $f_s = 28$ MHz, which is slightly higher than the minimum sampling rate $f_s \geq B = \max\{B_1, B_2, B_3\}$ required for perfect recovery of the power spectrum of the wide frequency band. The SNR is set to 5 dB. Fig. 4(a) shows the true (marked with '□') and the estimated (marked with '+') carrier frequencies and DoAs for the three sources. We can see that the estimated carrier frequencies and DoAs coincide with the groundtruth

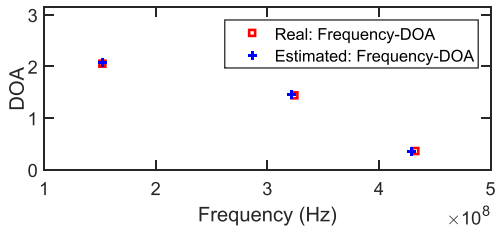

(a) True and estimated carrier frequencies and DoAs.

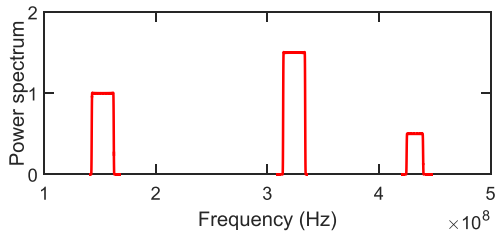

(b) Original power spectra of sources.

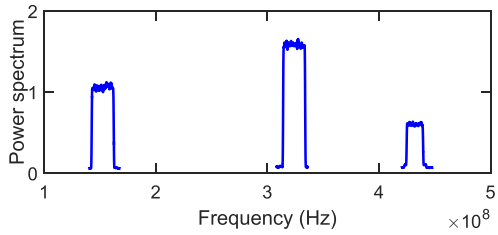

(c) Estimated power spectra of sources.

Fig. 4. True and estimated carrier frequencies, DoAs, and power spectra of sources, SNR = 5 dB.

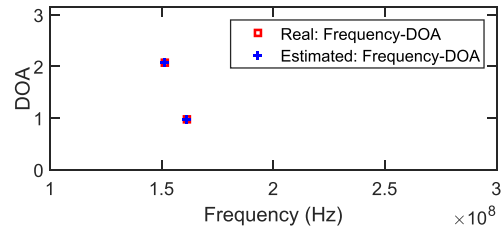

(a) True and estimated carrier frequencies and DoAs.

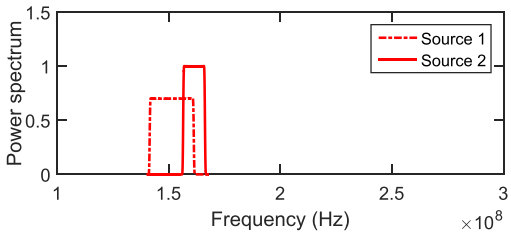

(b) Original power spectra of sources.

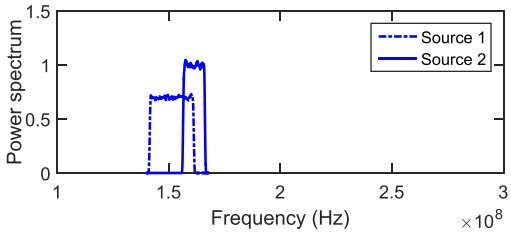

(c) Estimated power spectra of sources.

Fig. 5. Estimated carrier frequencies, DoAs and power spectra for sources that have partial spectral overlap, SNR = 20 dB.

well. Fig. 4(b) and 4(c) respectively depict the original power spectrum and the estimated power spectrum of the wide frequency band. It can be observed that our proposed method, even with a low SNR and a sampling rate far below the Nyquist rate, is able to accurately identify the locations of the occupied bands.

Next, we examine the scenario where frequency bands of the narrowband sources overlap each other. Set $K = 2$. The DoAs of these two sources are given respectively by $\theta_1 = 2.064$ and $\theta_2 = 0.968$. The carrier frequencies and bandwidths associated with these two sources are set to $f_1 = 151.36\,\text{MHz}$, $f_2 = 161.36\,\text{MHz}$, $B_1 = 20\,\text{MHz}$, and $B_2 = 10\,\text{MHz}$. The power spectra associated with the two sources are shown in Fig. 5(b), from which we can see that the two sources partially overlap in the frequency domain. The number of data samples N_s and the sampling rate f_s remain the same as in the previous example. The SNR is set to 20 dB. The estimated carrier frequencies, DoAs, and the power spectra of the two sources are plotted in Fig. 5(a) and 5(c). We see that our proposed method works well for sources with partially overlapping frequency bands. This example shows that our proposed method not only can perform wideband spectrum sensing, but also has the ability to blindly separate power spectra of sources that have partial spectral overlap.

To better evaluate the performance of our proposed method, we calculate the mean square errors (MSEs) for the following sets of parameters $\{\boldsymbol{\xi}, \boldsymbol{\psi}, \boldsymbol{\theta}\}$: $\text{MSE}(\psi) = \sum_{k=1}^{K} |\psi_k - \hat{\psi}_k|^2$, $\text{MSE}(\xi) = \sum_{k=1}^{K} |\xi_k - \hat{\xi}_k|^2$, and $\text{MSE}(\theta) = \sum_{k=1}^{K} |\theta_k - \hat{\theta}_k|^2$. Recalling that in our analysis, instead of concerning $\{\theta_k, \omega_k\}$, we define two new parameters $\xi_k \triangleq \omega_k \tau_k$ and $\psi_k \triangleq \omega_k / c$ and derive the CRB for $\{\xi_k, \psi_k\}$ in order to avoid the numerical instability issue. The estimation accuracy of the carrier frequencies is quantified by the normalized mean square error (NMSE) defined as $\text{NMSE}\,(\boldsymbol{\omega}) = \sum_{k=1}^{K} |\omega_k - \hat{\omega}_k|^2 / |\omega_k|^2$. We compare our proposed method, referred to as the CP-PASS-FD, with other sub-Nyquist sampling-based joint angle and carrier frequency estimation methods, namely, the joint-ESPRIT algorithm developed in the CaSCADE framework (referred to as CaSCADE) [20], and the two-dimensional multi-resolution algorithm (denoted as 2DMR) developed in a time delay-based sub-Nyquist sampling framework [18]. In [18], each antenna is followed by two sampling channels. To make a fair comparison, we assume $N = 4$ for [18] such that its number of sampling channels is identical to that of our architecture. In [20], an L-shape array is employed and its total number of antennas is $2T - 1$, where T denotes the number of antennas along each axis. Here we assume $T = 5$. Thus the total number of sampling channels for [20] is 9, which is slightly larger than our method and [18]. Also, the sampling rate per channel, f_s, is assumed to be the same for all these three methods. In addition, the competing algorithms [18], [20] require the knowledge of the number of source signals, K. Hence, for a fair comparison, we assume that the knowledge of K is available to all algorithms in our experiments.

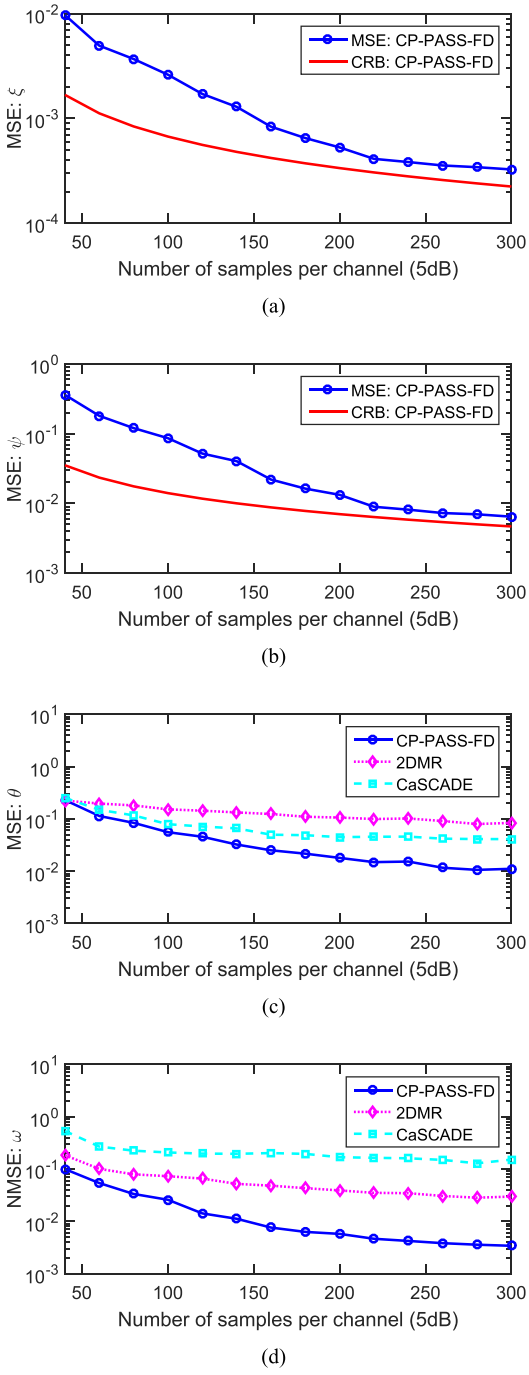

Fig. 6. MSEs and NMSE vs. the number of samples per channel, where $N = 8$ and SNR $= 5$ dB.

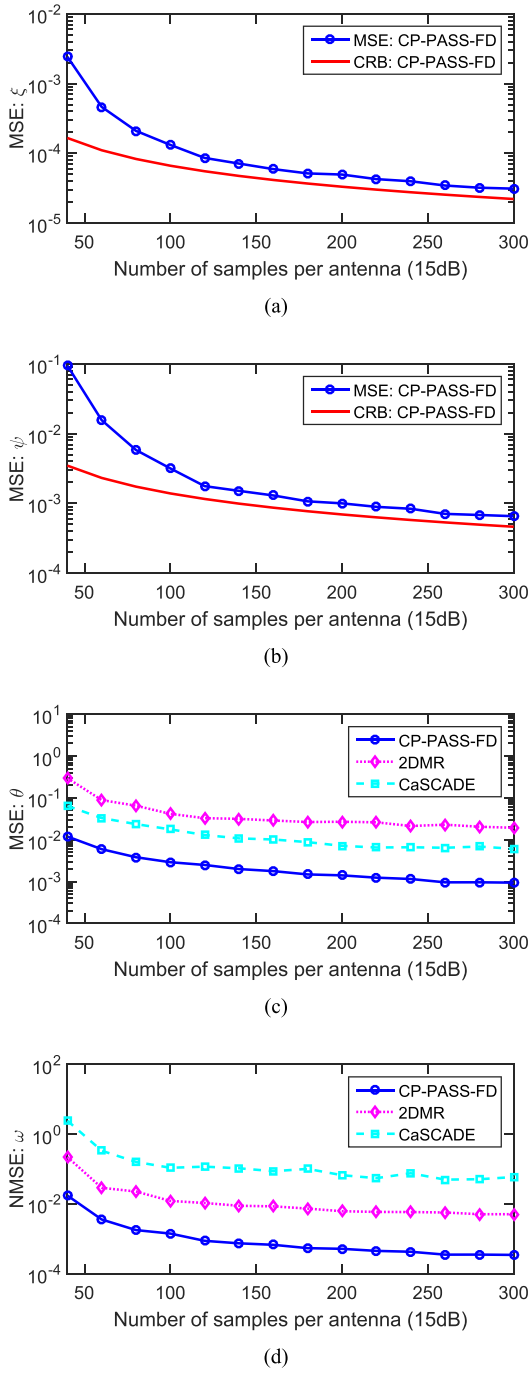

Fig. 7. MSEs and NMSE vs. the number of samples per channel, where $N = 8$ and SNR $= 15$ dB.

In this example, we set the number of sources $K = 2$. The parameters associated with these two sources are given as: $f_1 = 152$ MHz, $f_2 = 437$ MHz, $B_1 = 126$ KHz, $B_2 = 63$ KHz, $\theta_1 = \pi/4$, and $\theta_2 = \pi/3$. The sampling rate is set to $f_s = 1.26$ MHz. Figs. 6 and 7 depict the MSEs/NMSEs of respective sets of parameters vs. the number of samples N_s per channel, where we set SNR $= 5$ dB and SNR $= 15$ dB, respectively. MSE/NMSE results are averaged over 1000 independent runs, where the baseband complex source signals are randomly generated for each run. We see that our proposed method can achieve an estimation accuracy close to the CRBs by using only a small number of data samples, e.g. $N_s = 200$. From Fig. 6(c)–(d) and Fig. 7(c)–(d), it can be observed that our proposed method achieves a much higher carrier frequency and DoA estimation accuracy than the other two methods. This performance improvement is primarily due to the fact that our proposed method utilizes both spatial and temporal correlations of received signals (i.e. correlation matrices with different time lags), whereas the temporal correlation was neglected in the other two methods. We also observe that the CaSCADE achieves a higher DoA estimation accuracy than the 2DMR, whereas the 2DMR obtains a more accurate carrier frequency estimate than the CaSCADE.

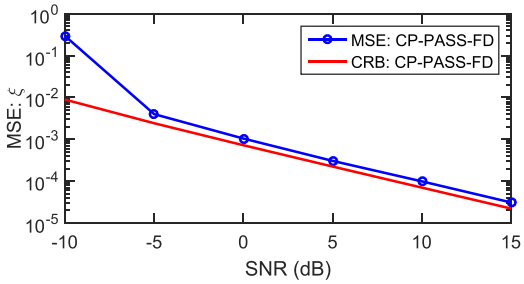

(a)

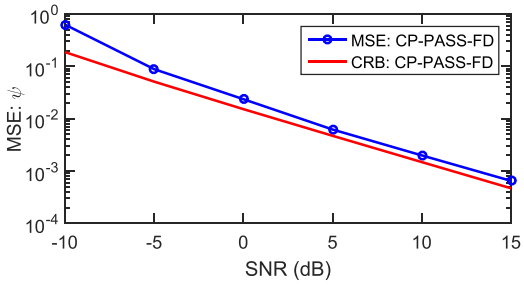

(b)

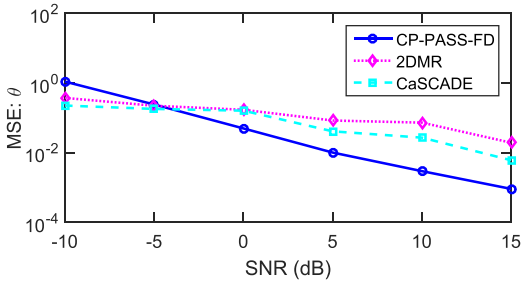

(c)

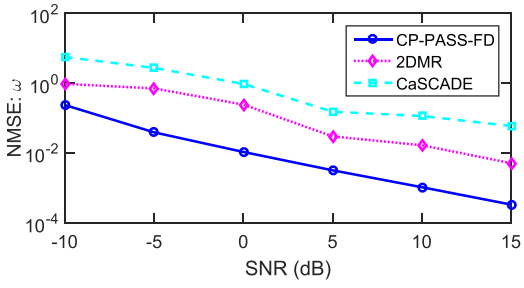

(d)

Fig. 8. MSEs and NMSE vs. SNR (dB), where $N = 8$ and $N_s = 300$.

This is because the CaSCADE and the 2DMR have different orders in their estimation processes. For the 2DMR, the carrier frequencies are estimated first and then the DoAs are extracted based on the estimated carrier frequencies. For the CaSCADE, the order is reversed, with the DoAs estimated first and then the carrier frequencies. Due to the error propagation, the parameters estimated in the latter stage incur larger estimation errors. In Fig. 8, we plot the MSEs/NMSEs of different sets of parameters as a function of the SNR, where $N_s = 300$ data samples per channel are used. We see that our proposed method outperforms the other two methods for most cases, and attains an accurate estimate of the DoAs/carrier frequencies with the MSE (NMSE) as low as 10^{-3} under a moderately high SNR.

IX. Conclusion

We considered the problem of joint wideband spectrum sensing and DoA estimation in this paper. To overcome the sampling rate bottleneck, we proposed a phased-array based sub-Nyquist sampling architecture that is simpler in structure and easier for implementation as compared with existing sub-Nyquist receiver architectures. Based on the proposed receiver architecture, we developed a CP decomposition-based method for joint DoA, carrier frequency, and power spectrum estimation. The conditions for exact recovery of the parameters and the power spectrum were analyzed. Our analysis suggests that the perfect recovery condition for our proposed method is mild: to recover the power spectrum of the wide frequency band, we only need the sampling rate to be greater than the bandwidth of the narrowband source signal which has the largest bandwidth among all sources. In addition, even for the case where sources have partial spectral overlap, our proposed method is still able to extract the DoA, carrier frequency, and the power spectrum associated with each source signal. CRB analysis for our estimation problem was also carried out. Simulation results show that our proposed method, with only a small number of data samples, can achieve an estimation accuracy close to the associated CRBs.

References

[1] E. Axell, G. Leus, E. G. Larsson, and H. V. Poor, "Spectrum sensing for cognitive radio: State-of-the-art and recent advances," *IEEE Signal Process. Mag.*, vol. 29, no. 3, pp. 101–116, May 2012.
[2] H. Sun, A. Nallanathan, C.-X. Wang, and Y. Chen, "Wideband spectrum sensing for cognitive radio networks: A survey," *IEEE Wireless Commun.*, vol. 20, no. 2, pp. 74–81, Apr. 2013.
[3] M. Mishali and Y. C. Eldar, "Blind multiband signal reconstruction: Compressed sensing for analog signals," *IEEE Trans. Signal Process.*, vol. 57, no. 3, pp. 993–1009, Mar. 2009.
[4] M. Mishali and Y. C. Eldar, "From theory to practice: Sub-Nyquist sampling of sparse wideband analog signals," *IEEE J. Sel. Topics Signal Process.*, vol. 4, no. 2, pp. 375–391, Apr. 2010.
[5] M. Mishali, Y. C. Eldar, O. Dounaevsky, and E. Shoshan, "Xampling: Analog to digital at sub-Nyquist rates," *IET Circuits, Devices Syst.*, vol. 5, no. 1, pp. 8–20, Jan. 2011.
[6] M. Wakin *et al.*, "A nonuniform sampler for wideband spectrally-sparse environments," *IEEE J. Emerg. Sel. Topics Circuits Syst.*, vol. 2, no. 3, pp. 516–529, Sep. 2012.
[7] E. Candés, J. Romberg, and T. Tao, "Robust uncertainty principles: Exact signal reconstruction from highly incomplete frequency information," *IEEE Trans. Inf. Theory*, vol. 52, no. 2, pp. 489–509, Feb. 2006.
[8] D. L. Donoho, "Compressive sensing," *IEEE Trans. Inf. Theory*, vol. 52, no. 4, pp. 1289–1306, Apr. 2006.
[9] D. D. Ariananda and G. Leus, "Compressive wideband power spectrum estimation," *IEEE Trans. Signal Process.*, vol. 60, no. 9, pp. 4775–4789, Sep. 2012.
[10] C.-P. Yen, Y. Tsai, and X. Wang, "Wideband spectrum sensing based on sub-Nyquist sampling," *IEEE Trans. Signal Process.*, vol. 61, no. 12, pp. 3028–3040, Jun. 2013.
[11] D. Cohen and Y. C. Eldar, "Sub-Nyquist sampling for power spectrum sensing in cognitive radios: A unified approach," *IEEE Trans. Signal Process.*, vol. 62, no. 15, pp. 3897–3910, Aug. 2014.
[12] M. D. Zoltowski and C. P. Mathews, "Real-time frequency and 2-D angle estimation with sub-Nyquist spatio-temporal sampling," *IEEE Trans. Signal Process.*, vol. 42, no. 10, pp. 2781–2794, Oct. 1994.
[13] S. Stein, O. Yair, D. Cohen, and Y. C. Eldar, "Joint spectrum sensing and direction of arrival recovery from sub-Nyquist samples," in *Proc. IEEE Int. Workshop Signal Process. Adv. Wireless Commun.*, Stockholm, Sweden, 2015, pp. 331–335.

[14] A. N. Lemma, A.-J. van der Veen, and E. F. Deprettere, "Joint angle-frequency estimation using multi-resolution ESPRIT," in *Proc. IEEE Int. Conf. Acoust., Speech, Signal Process.*, Seattle, WA, USA, 1998, pp. 1957–1960.
[15] A. N. Lemma, A.-J. van der Veen, and E. F. Deprettere, "Analysis of joint angle-frequency estimation using ESPRIT," *IEEE Trans. Signal Process.*, vol. 51, no. 5, pp. 1264–1283, May 2003.
[16] J.-D. Lin, W.-H. Fang, Y.-Y. Wang, and J.-T. Chen, "FSF MUSIC for joint DOA and frequency estimation and its performance analysis," *IEEE Trans. Signal Process.*, vol. 54, no. 12, pp. 4529–4542, Dec. 2006.
[17] D. D. Ariananda and G. Leus, "Compressive joint angular-frequency power spectrum estimation," in *Proc. IEEE Eur. Signal Process. Conf.*, Marrakech, Morocco, 2013, pp. 1–5.
[18] A. A. Kumar, S. G. Razul, and C.-M. S. See, "An efficient sub-Nyquist receiver architecture for spectrum blind reconstruction and direction of arrival estimation," in *Proc. IEEE Int. Conf. Acoust., Speech, Signal Process.*, Florence, Italy, 2014, pp. 6781–6785.
[19] A. A. Kumar, S. G. Razul, and C.-M. S. See, "Spectrum blind reconstruction and direction of arrival estimation at sub-Nyquist sampling rates with uniform linear array," in *Proc. IEEE Int. Conf. Digit. Signal Process.*, Singapore, 2015, pp. 670–674.
[20] S. S. Ioushua, O. Yair, D. Cohen, and Y. C. Eldar, "CaSCADE: Compressed carrier and DOA estimation," *IEEE Trans. Signal Process.*, vol. 65, no. 10, pp. 2645–2658, May 2017.
[21] C. Cui, W. Wu, and W. Q. Wang, "Carrier frequency and DOA estimation of sub-Nyquist sampling multi-band sensor signals," *IEEE Sensors J.*, vol. 17, no. 22, pp. 7470–7478, Nov. 2017.
[22] L. Liu and P. Wei, "Joint DOA and frequency estimation with sub-Nyquist sampling," 2016, arXiv:1604.05037.
[23] T. G. Kolda and B. W. Bader, "Tensor decompositions and applications," *SIAM Rev.*, vol. 51, no. 3, pp. 455–500, 2009.
[24] A. Lavrenko *et al.*, "Spatially resolved sub-Nyquist sensing of multiband signals with arbitrary antenna arrays," in *Proc. IEEE Int. Workshop Signal Process. Adv. Wireless Commun.*, Edinburgh, U.K., 2016, pp. 1–5.
[25] H. Akaike, "A new look at the statistical model identification," *IEEE Trans. Autom. Control*, vol. AC-19, no. 6, pp. 716–723, Dec. 1974.
[26] J. A. Bazerque, G. Mateos, and G. B. Giannakis, "Rank regularization and Bayesian inference for tensor completion and extrapolation," *IEEE Trans. Signal Process.*, vol. 61, no. 22, pp. 5689–5703, Nov. 2013.
[27] P. Rai, Y. Wang, S. Guo, G. Chen, D. Dunson, and L. Carin, "Scalable Bayesian low-rank decomposition of incomplete multiway tensors," in *Proc. 31st Int. Conf. Mach. Learn.*, Beijing, China, 2014, vol. 32, pp. 1800–1808.
[28] Q. Zhao, L. Zhang, and A. Cichocki, "Bayesian CP factorization of incomplete tensors with automatic rank determination," *IEEE Trans. Pattern Anal. Mach. Intell.*, vol. 37, no. 9, pp. 1751–1763, Sep. 2015.
[29] J. B. Kruskal, "Three-way arrays: Rank and uniqueness of trilinear decompositions, with application to arithmetic complexity and statistics," *Linear Algebra Appl.*, vol. 18, no. 2, pp. 95–138, 1977.
[30] A. Stegeman and N. D. Sidiropoulos, "On Kruskal's uniqueness condition for the Candecomp/Parafac decomposition," *Linear Algebra Appl.*, vol. 420, no. 2/3, pp. 540–552, Jan. 2007.
[31] R. A. Harshman, "Determination and proof of minimum uniqueness conditions for PARAFAC1," *UCLA Work. Papers Phonetics*, vol. 22, pp. 111–117, 1972.
[32] P. Pal and P. P. Vaidyanathan, "Nested arrays: A novel approach to array processing with enhanced degrees of freedom," *IEEE Trans. Signal Process.*, vol. 58, no. 8, pp. 4167–4181, Aug. 2010.
[33] P. P. Vaidyanathan and P. Pal, "Sparse sensing with co-prime samplers and arrays," *IEEE Trans. Signal Process.*, vol. 59, no. 2, pp. 573–586, Feb. 2011.
[34] K. V. Mishra, I. Kahane, A. Kaufmann, and Y. C. Eldar, "High spatial resolution radar using thinned arrays," in *Proc. IEEE Radar Conf.*, Seattle, WA, USA, 2017, pp. 1119–1124.
[35] S. M. Kay, *Fundamentals of Statistical Signal Processing: Estimation Theory*. Upper Saddle River, NJ, USA: Prentice-Hall, 1993.
[36] P. Stoica and A. Nehorai, "Performance study of conditional and unconditional direction-of-arrival estimation," *IEEE Trans. Acoust., Speech, Signal Process.*, vol. 38, no. 10, pp. 1783–1795, Oct. 1990.
[37] P. Stoica, E. G. Larsson, and A. B. Gershman, "The stochastic CRB for array processing: A textbook derivation," *IEEE Signal Process. Lett.*, vol. 8, no. 5, pp. 148–150, May 2001.

Feiyu Wang received the B.Sc. degree from Zhejiang Ocean University, Zhoushan, China, in 2011, and the M.Sc. degree from Ningbo University, Ningbo, China, in 2014, both in electrical engineering. Since August 2014, he has been working toward the Ph.D. degree in electrical engineering with the University of Electronic Science and Technology of China, Chengdu, China. His current research interests include compressed sensing, tensor analysis, and statistical signal processing.

Jun Fang (M'08) received the B.S. and M.S. degrees from Xidian University, Xi'an, China, in 1998 and 2001, respectively, and the Ph.D. degree from the National University of Singapore, Singapore, in 2006, all in electrical engineering.

During 2006, he was a Postdoctoral Research Associate with the Department of Electrical and Computer Engineering, Duke University. From January 2007 to December 2010, he was a Research Associate with the Department of Electrical and Computer Engineering, Stevens Institute of Technology. Since 2011, he has been with the University of Electronic Science and Technology of China, Chengdu, China. His research interests include compressed sensing and sparse theory, massive MIMO/mmWave communications, and statistical inference.

Dr. Fang was the recipient of the IEEE Jack Neubauer Memorial Award in 2013 for the best systems paper published in the IEEE TRANSACTIONS ON VEHICULAR TECHNOLOGY. He is a Senior Associate Editor for the IEEE SIGNAL PROCESSING LETTERS.

Huiping Duan received the B.S. and M.S. degrees from Xidian University, Xi'an, China, in 1998 and 2001, respectively, and the Ph.D. degree in electrical engineering from Nanyang Technological University, Singapore, in 2008. Since 2011, she has been with the University of Electronic Science and Technology of China, Chengdu, China, where she is currently an Associate Professor. Her research interests include compressed sensing and sparse theory, array signal processing, and statistical inference.

Hongbin Li (M'99–SM'08) received the B.S. and M.S. degrees from the University of Electronic Science and Technology of China, Chengdu, China, in 1991 and 1994, respectively, and the Ph.D. degree from the University of Florida, Gainesville, FL, USA, in 1999, all in electrical engineering.

From July 1996 to May 1999, he was a Research Assistant with the Department of Electrical and Computer Engineering, University of Florida. Since July 1999, he has been with the Department of Electrical and Computer Engineering, Stevens Institute of Technology, Hoboken, NJ, USA, where he became a Professor in 2010. He was a Summer Visiting Faculty Member with the Air Force Research Laboratory in the summers of 2003, 2004, and 2009. His general research interests include statistical signal processing, wireless communications, and radars.

Dr. Li was the recipient of the IEEE Jack Neubauer Memorial Award in 2013 from the IEEE Vehicular Technology Society, the Outstanding Paper Award from the IEEE AFICON Conference in 2011, the Harvey N. Davis Teaching Award in 2003 and the Jess H. Davis Memorial Award for excellence in research in 2001 from Stevens Institute of Technology, and the Sigma Xi Graduate Research Award from the University of Florida in 1999. He has been a member of the IEEE SPS Signal Processing Theory and Methods Technical Committee (TC) and the IEEE SPS Sensor Array and Multichannel TC, an Associate Editor for *Signal Processing* (Elsevier), the IEEE TRANSACTIONS ON SIGNAL PROCESSING, the IEEE SIGNAL PROCESSING LETTERS, and the IEEE TRANSACTIONS ON WIRELESS COMMUNICATIONS, as well as a Guest Editor for the IEEE JOURNAL OF SELECTED TOPICS IN SIGNAL PROCESSING and the *EURASIP Journal on Applied Signal Processing*. He has been involved in various conference organization activities, including serving as a General Co-Chair for the 7th IEEE Sensor Array and Multichannel Signal Processing Workshop, Hoboken, NJ, USA, June 17–20, 2012. He is a member of Tau Beta Pi and Phi Kappa Phi.